Turning Ocean Mixing Upside Down

RAFFAELE FERRARI AND ALI MASHAYEK

Massachusetts Institute of Technology, Cambridge, Massachusetts

TREVOR J. MCDOUGALL

School of Mathematics and Statistics, University of New South Wales, Sydney, New South Wales, Australia

MAXIM NIKURASHIN

Institute for Marine and Antarctic Studies, University of Tasmania, Hobart, Tasmania, and ARC Centre of Excellence for Climate System Science, Sydney, New South Wales, Australia

JEAN-MICHAEL CAMPIN

Massachusetts Institute of Technology, Cambridge, Massachusetts

(Manuscript received 9 December 2015, in final form 14 April 2016)

ABSTRACT

It is generally understood that small-scale mixing, such as is caused by breaking internal waves, drives upwelling of the densest ocean waters that sink to the ocean bottom at high latitudes. However, the observational evidence that the strong turbulent fluxes generated by small-scale mixing in the stratified ocean interior are more vigorous close to the ocean bottom boundary than above implies that small-scale mixing converts light waters into denser ones, thus driving a net sinking of abyssal waters. Using a combination of theoretical ideas and numerical models, it is argued that abyssal waters upwell along weakly stratified boundary layers, where small-scale mixing of density decreases to zero to satisfy the no density flux condition at the ocean bottom. The abyssal ocean meridional overturning circulation is the small residual of a large net sinking of waters, driven by small-scale mixing in the stratified interior above the bottom boundary layers, and a slightly larger net upwelling, driven by the decay of small-scale mixing in the boundary layers. The crucial importance of upwelling along boundary layers in closing the abyssal overturning circulation is the main finding of this work.

1. Introduction

The abyssal meridional overturning circulation is fed by waters that become dense enough to sink into the ocean abyss at high latitudes and return to the surface through convoluted three-dimensional pathways. While it is well established that most of the sinking is confined to the Labrador and Greenland Seas in the North Atlantic and the Weddell and Ross Seas around Antarctica, the return pathways are less understood (Talley et al. 2011). The consensus is that widespread small-scale mixing generated by breaking internal waves provides most of the energy to lift the North Atlantic Deep Waters (NADWs) and the Antarctic Bottom Waters (AABWs) up to a depth of approximately 2000 m; internal waves break within a few hundred meters of abyssal ridges, mountains, and rises, which are most ubiquitous below 2000 m (Munk 1966; Ferrari 2014). Once the waters rise above 2000 m, they flow southward along density surfaces to the Southern Ocean, where the Roaring Forties lift them to the surface to be transformed into intermediate waters that flow back toward Antarctica and the North Atlantic, thereby closing the overturning loop [see the review by Marshall and Speer (2012)]. There would appear to be a

Corresponding author address: Raffaele Ferrari, Massachusetts Institute of Technology, 77 Massachusetts Ave., Cambridge, MA 02139.
E-mail: rferrari@mit.edu

DOI: 10.1175/JPO-D-15-0244.1

major inconsistency in this scenario: strong internal wave–driven mixing is typically bottom intensified and thus drives sinking, not rising, of waters through density surfaces (e.g., St. Laurent et al. 2001; Klocker and McDougall 2010). In this paper, the conundrum is resolved by arguing that abyssal waters come to the surface along turbulent bottom boundary layers, rather than in the stratified ocean interior.

We begin by establishing a few well-documented observations about the ocean. First, the ocean is stably stratified on time scales longer than a few hours (e.g., Talley et al. 2011). Second, estimates of the zonally averaged global overturning circulation based on inverse calculations from ocean observations (Ganachaud and Wunsch 2000; Lumpkin and Speer 2007) and numerical models constrained to observations (Wunsch and Heimbach 2009) show that waters sink to the ocean bottom at high latitudes and then slowly rise throughout the rest of the oceans crossing density surfaces at least up to 2000 m (Marshall and Speer 2012; Talley 2013). Third, there is growing evidence from in situ measurements that the turbulent kinetic energy generated by breaking internal waves is large within a few hundred meters of rough-bottom topography and decays to weaker values farther up in the water column. The bottom enhancement of turbulence reflects the generation of energetic waves by tides and geostrophic flows impinging over topography and breaking locally (e.g., Wunsch and Ferrari 2004; Garrett and Kunze 2007; Nikurashin and Ferrari 2013). During a breaking event most of the energy is lost to dissipation, but a fraction is expended in mixing the stratified fluid (Osborn 1980). Mixing rates have been estimated to be two to three orders of magnitude above interior levels within a few hundred meters of rough ocean topography (Polzin et al. 1997; St. Laurent et al. 2012). The term mixing is used here to refer to the turbulent density flux generated by breaking waves and not the turbulent diffusivity, which is equal to minus the turbulent flux divided by the density stratification. A recent comprehensive compilation of available mixing profiles confirms that ocean mixing rates are stronger within a kilometer of rough ocean bottom topography and weaker above, while mixing rates are weak and nearly uniform above smooth topography (Waterhouse et al. 2014).

The emerging evidence that mixing increases toward the ocean bottom, at least above rough topography where mixing is strong and contributes significantly to water mass transformations, represents the key departure from the textbook explanation of how mixing contributes to waters rising from the abyss (Munk 1966; Munk and Wunsch 1998). Waters that sink to the abyss along Antarctica flood the ocean below 2000 m. Munk (1966) argued that these abyssal waters are transformed into lighter waters in the ocean interior as a result of internal wave–driven mixing. However, waters sink (they do not rise) in regions where the rate of mixing increases toward the ocean bottom (Gargett 1984; Polzin et al. 1997; St. Laurent et al. 2001; Simmons et al. 2004; Klocker and McDougall 2010; Kunze et al. 2012). The goal of this paper is to resolve the conundrum of how bottom waters are transformed into lighter waters. We will argue that abyssal waters rise toward the surface as lighter waters in narrow turbulent boundary layers that develop along the continental margins and abyssal ridges.

This paper focuses on the diabatic transformation of abyssal water masses, that is, the part of the overturning circulation that crosses density surfaces. The global transport of tracers like heat and freshwater is affected by additional flows along density surfaces, like isopycnal stirring and mixing by geostrophic eddies, which will not be discussed. Our approach is similar to the one taken by Nikurashin and Ferrari (2013) and by de Lavergne et al. (2016), who studied the role of mixing in driving water mass transformations in the deep ocean using available estimates of internal wave–driven mixing. But our focus is on understanding and quantifying the crucial role played by the turbulent bottom boundary layers.

The paper is organized as follows. In section 2, we use heuristic and formal arguments to explain why a bottom enhancement of abyssal mixing results in diapycnal sinking of waters in the stratified ocean interior and diapycnal rising of waters along bottom boundary layers. Section 3 introduces the idealized numerical model used to test our theory. In section 4, we use the numerical model to illustrate how ocean mixing and the shape of bathymetry affect the abyssal ocean overturning circulation and stratification. We then show in section 5 that our claim that abyssal waters rise along deep sloping boundaries is supported by estimates of mixing profiles in the global ocean. Finally, in section 6, we conclude.

2. Theory

There is a rich literature on the role of mixing on water mass transformations in the ocean interior [see references in Wunsch and Ferrari (2004)]. Much work has also been done on mixing-driven flows along sloping boundary layers (e.g., Armi 1978; Garrett et al. 1993). However, the two lines of research have proceeded largely independently of each other. In this section we use Walin's (1982) approach to emphasize the connection between upwelling along sloping

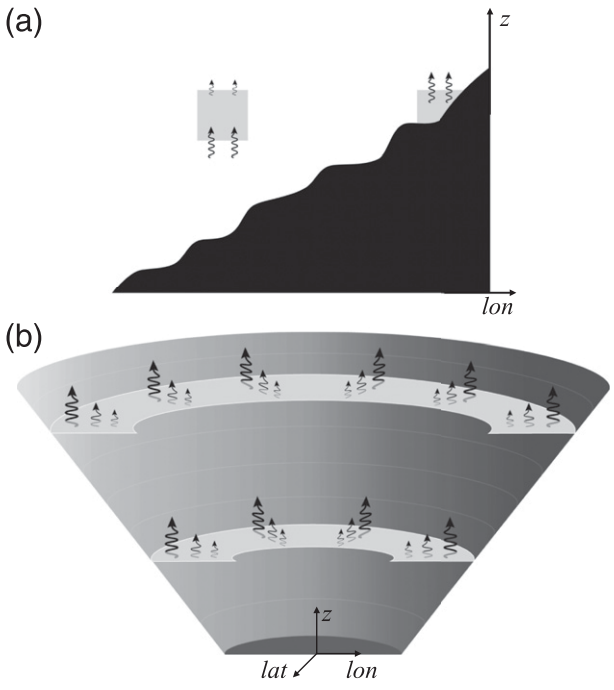

FIG. 1. (a) A longitude–depth section of the ocean above a sloping rough-bottom topography. A water parcel way above the ocean bottom boundary layer (left gray square) experiences more diapycnal mixing of density through its lower face than through its upper one as a result of the bottom enhancement of mixing. Mixing is represented as black curly arrows, whose length is proportional to the strength of mixing. This water parcel becomes denser and sinks in response to mixing. A water parcel sitting right on the ocean bottom topography (right gray square) experiences mixing only through its upper surface. This water parcel becomes lighter and rises in response to mixing. (b) A cut through a conical ocean basin with area increasing toward the surface. The two light gray horizontal stripes along the ocean boundary represent two density surfaces. Only the portion of the density surfaces experiencing strong mixing in the near-boundary region is shown. As the upper surface is larger than the lower one, the mixing integrated over the upper surface may exceed that integrated on the lower surface, even though mixing increases toward the ocean bottom along every vertical profile (before going to zero right at the ocean bottom).

boundaries and interior sinking in response to bottom-intensified mixing.

We begin our discussion with an illustrative example. Consider the schematic in Fig. 1a. A water parcel in the middle of the ocean water column, sketched as a gray square, experiences stronger mixing through its lower face than its upper face, consistent with the observational evidence that vertical mixing is stronger at depth. Mixing will make this water parcel denser by diffusing more heavy waters from below than light waters from above. A mixing profile that increases toward the ocean bottom acts to increase the density of water parcels. (We consider only mixing in the vertical because in the ocean interior the diapycnal direction is very close to vertical.)

To understand how water parcels rise to the surface as lighter waters, one must consider what happens close to the ocean solid boundaries. Mixing vanishes right at the seafloor because ocean turbulence does not mix density across the solid boundary. Thus, the rate of mixing drops to zero within a thin boundary layer close to the ocean bottom. The parcel in the bottom boundary layer (BBL) sketched in Fig. 1a experiences mixing only on its upper face and becomes lighter. The implication of this simple thought experiment is that water parcels are transformed into heavier density classes in the stratified ocean interior, while they are transformed into lighter density classes along the oceanic boundaries.

Figure 1b depicts a hypothetical conical ocean basin, where the area of the basin decreases with depth. The two horizontal strips along the ocean boundary represent two constant density surfaces, taken to be flat for simplicity. (The density surfaces should tilt and intersect the boundary at right angles within the narrow BBL, but this correction is irrelevant in this example.) The horizontal strips represent the portions of the density surfaces that experience the strong near-boundary mixing. If the width of the strips is constant with depth, then the area of the upper strip is larger than that of the lower strip because of the shape of the ocean topography. Thus, the mixing integrated over the upper density surface can be larger than the mixing integrated over the lower density surface, even though mixing increases toward the bottom in every vertical profile. Whether the whole volume between the two density surfaces is mixed more with the waters above or below will depend on the relative rate at which the ocean area experiencing mixing decreases with depth versus the rate at which mixing increases with depth. It is important to remark that what matters is the rate of change of the near-boundary area experiencing mixing and not the rate of change of the whole ocean area (the hypsometry).

This heuristic argument can be cast in more rigorous mathematical terms. The equation for the mass transport across a density surface in the ocean interior is derived in McDougall (1984) for seawater, which has an equation of state that depends nonlinearly on temperature, salinity, and pressure. Here, we will consider the simpler case of a linear equation of state, which is sufficient to study the qualitative aspects of mixing-driven flows. The reader is referred to the recent paper by de Lavergne et al. (2016) for a discussion of the mass transport generated by mixing in the abyssal ocean with a nonlinear equation of state. Our goal is to illustrate how interior mixing drives both downwelling across density surfaces in the ocean interior and upwelling along the boundaries, rather than providing an accurate estimate of the observed ocean overturning circulation.

The equation for the conservation of density, ignoring nonlinearities in the equation of state, averaged on time scales longer than a few hours and spatial scales larger than a hundred meters, that is, scales larger than those at which isopycnals are overturned by breaking waves or boundary layer turbulence, is

$$\frac{\partial \rho}{\partial t} + \mathbf{v} \cdot \nabla \rho = -\nabla \cdot \mathbf{F}_\rho, \tag{1}$$

where $\mathbf{F}_\rho = \overline{\mathbf{v}'\rho'}$ is the turbulent density flux due to correlations between velocity and density fluctuations on time scales shorter than the averaging scales denoted by the overbar. The diapycnal velocity across a density surface (equivalent to a buoyancy surface or isopycnal for a linear equation of state) differs from the Eulerian velocity normal to the isopycnal because the isopycnal itself moves through the fluid. The Eulerian velocity normal to an isopycnal is $\mathbf{v} \cdot \mathbf{n}_\rho$, where $\mathbf{n}_\rho$ is the unit vector normal to the isopycnal. The velocity of an isopycnal surface, say $\mathbf{v}_\rho$, in the direction normal to itself is (Marshall et al. 1999)

$$\mathbf{v}_\rho \equiv -\frac{1}{|\nabla \rho|} \frac{\partial \overline{\rho}}{\partial t} \mathbf{n}_\rho. \tag{2}$$

To calculate the diapycnal velocity $\tilde{\mathbf{e}}$, we must accordingly subtract $\mathbf{v}_\rho$ from the Eulerian velocity:

$$\tilde{\mathbf{e}} \equiv (\mathbf{v} \cdot \mathbf{n}_\rho)\mathbf{n}_\rho - \mathbf{v}_\rho = -\frac{\nabla \cdot \mathbf{F}_\rho}{|\nabla \rho|} \mathbf{n}_\rho. \tag{3}$$

This expression for the full diapycnal velocity, normal to the isopycnal, is derived, for example, in Marshall et al. (1999) but differs from the one reported in McDougall (1984) and de Lavergne et al. (2016), who only considered its vertical component. This difference is important when considering regions of weak vertical stratification like the turbulent BBLs.

Equation (3) confirms that a diapycnal velocity $\tilde{\mathbf{e}}$ develops only if there is a nonzero divergence of the turbulent flux of density, that is, if mixing is not homogeneous in space. (Technically molecular fluxes of heat and salt would still drive some cross-density transport, but this is so weak as to be irrelevant for present purposes.) Equation (3) holds only if the equation of state for density depends linearly on temperature and salinity, otherwise the diapycnal advection processes of cabbeling and thermobaricity need to be included (McDougall 1984). Klocker and McDougall (2010) showed that the global effect of both thermobaricity and cabbeling is to cause seawater to sink through isopycnals and thus reinforces the sinking induced by turbulent mixing in the ocean interior. We also assume that the turbulent density flux vanishes at the ocean bottom, thereby ignoring geothermal heat fluxes through the seafloor. These fluxes drive seawater to rise across isopycnals along the BBLs and reinforce the boundary upwelling of waters driven by turbulent mixing. Thus, both nonlinearities in the equation of state and geothermal heat flux act to reinforce the mixing-driven circulation described in this work.

In the stratified ocean interior, away from boundary layers, the vertical divergence of the turbulent density flux and the vertical gradient of density dominate over the horizontal components and, to a very good approximation, the diapycnal velocity is vertical and given by

$$\tilde{\mathbf{e}} \simeq \frac{1}{|\partial_z \rho|} \frac{\partial F_\rho^{(z)}}{\partial z} \mathbf{z}, \tag{4}$$

where $\mathbf{z}$ is the vertical unit vector and $\mathbf{n}_\rho \simeq -\mathbf{z}$. The turbulent density flux $F_\rho^{(z)}$ is typically positive (i.e., upward) in the ocean interior because in a stably stratified ocean turbulence tends to generate rising blobs of high density and sinking blobs of low density so that $F_\rho^{(z)} = \overline{w'\rho'} > 0$. In the following, we will refer to the turbulent flux $F_\rho^{(z)}$ as the mixing profile.

It is extremely difficult to directly measure the turbulent density flux in the ocean. Alternatively, oceanographers use the turbulent kinetic energy budget to infer $F_\rho^{(z)}$ in the stratified ocean interior away from boundaries. The rate at which a breaking wave loses its kinetic energy P is equal to the sum of the kinetic energy lost to heating through viscous dissipation ϵ plus the energy expended in changing the potential energy of the water column through mixing $F_\rho^{(z)}$:

$$P = \epsilon + F_\rho^{(z)}. \tag{5}$$

Osborn (1980) argued that in a stratified fluid mixed by breaking internal gravity waves the turbulent flux $F_\rho^{(z)}$ is a fraction of ϵ, that is, $F_\rho^{(z)} = \Gamma\epsilon$, where Γ is the mixing efficiency. Early measurements in the upper ocean (Gregg 1987) found that ϵ scaled with the local density stratification and thus increased toward the ocean surface. Assuming a constant mixing efficiency of $\Gamma = 0.2$, it was argued that the increase in $F_\rho^{(z)} = \Gamma\epsilon$ is consistent with the hypothesis that mixing is supported by the background wave field, which tends to be more energetic where the stratification is larger (Munk 1981). Most importantly, the observation that $\partial_z F_\rho^{(z)} > 0$ seemed to vindicate Munk's (1966) inference that mixing drives upwelling of waters through the stratified ocean.

Munk's (1966) picture came into question when the first measurements of dissipation in the abyssal ocean were collected as part of the Brazil Basin Experiment

(Polzin et al. 1997). The dissipation profiles of ϵ were found to increase by one to two orders of magnitude as the turbulent probes approached the ocean bottom above rough topography but were still in the stratified ocean above the BBL. Numerical simulations and laboratory experiments found that Γ varies within a factor of 2 of the canonical value of 0.2 (Smyth et al. 2001; Peltier and Caulfield 2003; Mashayek and Peltier 2013a). Mashayek and Peltier (2013b) further showed with numerical simulations that the neglect of nonlocal redistribution of energy in the Osborn (1980) model adds to the uncertainty in the estimate of $F_\rho^{(z)}$, but they concluded that the estimate $F_\rho^{(z)} = 0.2\epsilon$ is still within a factor of 3 of the true turbulent density flux. These uncertainties are sufficiently small that they do not affect the inference that $F_\rho^{(z)}$ increased by more than an order of magnitude toward the rough ocean bottom in the Brazil Basin Experiment. This result has now been confirmed by other observational campaigns (St. Laurent et al. 2012; Waterman et al. 2013; Waterhouse et al. 2014) and is supported by the evidence that this mixing is associated with breaking internal waves radiated from the ocean bottom. The turbulent density flux does indeed decrease with height above the BBL in regions of rough topography—energetic internal waves that break and mix close to topography are preferentially generated where the ocean bottom is rough—and results in a downward diapycnal velocity as per Eq. (4). Mixing is instead weak above smooth topography and does not contribute substantial diapycnal velocities. The dissipation measurements confirm that abyssal mixing above the BBL transforms light waters into denser waters and not the other way around.

The density flux does not increase all the way to the ocean bottom, because it must vanish at the solid boundary (or match the weak negative geothermal flux in the real ocean, thus reinforcing our result). The transition between the strong interior density flux and the zero value at the ocean boundaries occurs within a turbulent BBL, where the isopycnals become normal to the boundary so as to obey the no flux boundary condition. In the BBLs the dissipation of kinetic energy ϵ is large, whereas the density flux $F_\rho^{(z)}$ decays to zero. The mixing efficiency must therefore decrease to zero within the BBL in order for the turbulent density flux to go from its large value at the top of the BBL to zero at the solid boundary. Small mixing efficiencies are well documented in weakly stratified fluids (e.g., Bouffard and Boegman 2013; Karimpour and Venayagamoorthy 2014). In the limit of no stratification there can be no density flux regardless of the magnitude of ϵ. The BBL density flux divergence is dominated by the drop in flux normal to the boundary—lateral variations in the flux are much smaller[1]—and it is approximately equal to the ratio of turbulent flux at the top of the BBL divided by the depth of the BBL, which is a positive number. A positive $\nabla \cdot \mathbf{F}_\rho$ in Eq. (3) implies that along the BBLs the bottom waters are transformed from dense to light and rise toward the surface along the sloping seafloor. These along-boundary flows can thus balance the net sinking of waters in the ocean interior in response to the bottom-intensified mixing.

We will refer to the mixing-driven flows in the stratified interior and along the BBLs as diapycnal upwelling and downwelling. The diapycnal velocities are by definition normal to density surfaces. In the stratified interior, density surfaces are approximately horizontal and the diapycnal direction is vertical. In the BBL, density surfaces intersect the bottom boundary at normal angles and the diapycnal direction is along the solid boundary. The transformation of light waters into denser ones in the stratified interior is associated with a vertical downward velocity or diapycnal downwelling. The transformation of dense waters into lighter ones along the BBL is instead associated with an along-boundary flow as per Eq. (3). To the extent that the abyssal BBLs are sloped, this flow will have a vertical upward component, and we refer to it as a diapycnal upwelling. However, the "diapycnal upwelling" is horizontal if the BBL is flat.

To quantify whether the diapycnal upwelling along sloping BBLs is large enough to overcome the interior sinking and result in an overall net rising of waters across isopycnals, we must compute the net diapycnal transport across a density surface $A(\rho)$:

$$\mathcal{E}(\rho) \equiv -\iint_{A(\rho)} \tilde{\mathbf{e}} \cdot \mathbf{n}_\rho \, dA = \iint_{A(\rho)} \frac{\nabla \cdot \mathbf{F}_\rho}{|\nabla \rho|} dA \,, \qquad (6)$$

where we used the definition of diapycnal velocity in Eq. (3). The negative sign in front of the first integral is introduced to be consistent with the convention of defining a diapycnal transport to be positive when it goes from dense to light waters, that is, in the direction opposite to $\mathbf{n}_\rho$. We do not write it explicitly, but all transports and areas are understood to be time dependent. Our focus is on the transport generated by bottom-intensified mixing; thus, we will restrict the integral in Eq. (6) to the area $A_{\rm mix}(\rho)$,

[1] The divergence of the flux component normal to the boundary scales with $F_T^{(z)} \cos\theta/h$, where $F_T^{(z)}$ is the value of the vertical flux at the top of the BBL, θ is the slope of the topography, and h is the BBL thickness. Lateral variations of the flux contribute a divergence of order $F_T^{(z)} \sin\theta/L$, where L is the characteristic scale of along-boundary variations. Typical topographic slopes are less than $1/100$ and in boundary layers $h \ll L$; thus, $\nabla \cdot \mathbf{F}_\rho \sim F_T^{(z)} \cos\theta/h > 0$.

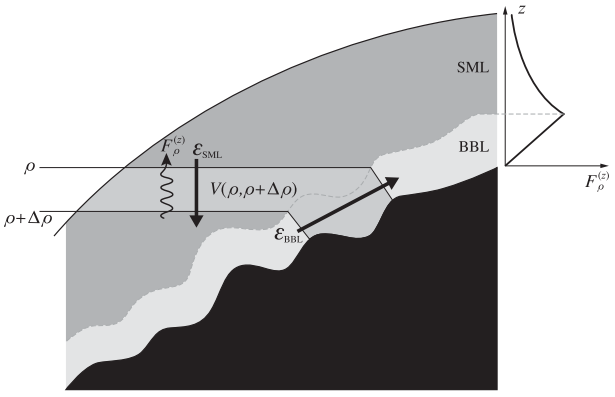

FIG. 2. A longitude–depth section of the near-boundary region of the ocean above rough topography is characterized by enhanced turbulence generated by tidal and geostrophic flows impinging over topography. The region closest to the boundary is characterized by a weakly stratified BBL a few tens of meters thick. Above the BBL, there is a SML, a region where topographically generated turbulence is still strong but not so strong as to substantially reduce the stratification. The combination of strong turbulence and large stratification results in a strong density flux $F_\rho^{(z)}$. The SML extends a few hundred meters in the vertical. A typical vertical profile of the turbulent density flux $F_\rho^{(z)}$ through the BBL and SML is sketched on the upper-right corner of the figure. The stratified ocean above the SML is characterized by weak turbulence rates. The shaded region $V(\rho, \rho + \Delta\rho)$, used in Walin's (1982) calculation of section 2, is circumscribed, vertically, by density surfaces ρ and $\rho + \Delta\rho$ and, laterally, by the outer edge of the SML and the ocean solid boundary. The black arrows indicate the diabatic sinking of waters in the SML and the diabatic along-boundary upwelling in the BBL.

that is, the near-boundary portion of the isopycnal that experiences the strong topographic mixing. As illustrated in Fig. 2, $A_{\rm mix}(\rho)$ includes both the portion of the isopycnal within the BBL, where mixing drives diabatic upwelling, and the portion of the isopycnal in the stratified interior, where mixing drives diabatic sinking. We will refer to the near-boundary region characterized by strong mixing, but excluding the BBL, as the stratified mixing layer (SML). While the BBL is of order of tens of meters thick (Weatherly and Martin 1978), the SML is a few hundred meters thick (e.g., Polzin et al. 1997; St. Laurent et al. 2012; Waterman et al. 2013). It is crucial that the integral is restricted to $A_{\rm mix}(\rho)$, otherwise $\mathcal{E}(\rho)$ would include additional diapycnal transports not relevant for a study of abyssal flows, like upper-ocean mixing and air–sea fluxes.

Walin (1982) developed an elegant framework to estimate the area integral in Eq. (6). Here, we follow the extensions of this approach described in Garrett et al. (1995) and Marshall et al. (1999). Using a generalized form of Leibniz's integral rule, the area integral is transformed into an integral over the control volume $V(\rho, \rho + \Delta\rho)$, sketched in Fig. 2, sandwiched between isopycnals ρ and $\rho + \Delta\rho$, in the limit $\Delta\rho \to 0$, and bounded laterally by the sloping ocean topography and the outer edge of the SML:

$$\mathcal{E}(\rho) = \lim_{\Delta\rho\to 0} \frac{1}{\Delta\rho} \iiint_{V(\rho,\rho+\Delta\rho)} \nabla\cdot\mathbf{F}_\rho \, dV. \tag{7}$$

Gauss's theorem states that the volume integral of a flux divergence is equal to the area integral of the flux across the bounding surface. The turbulent density flux normal to the outer edge of the SML is negligible by construction, and the flux into the solid boundary is zero (ignoring geothermal effects). Thus, the integral in Eq. (7) reduces to

$$\mathcal{E}(\rho) = \frac{\partial}{\partial\rho} \iint_{A_{\rm mix}(\rho)} \mathbf{F}_\rho\cdot\mathbf{n}_\rho \, dA \simeq -\frac{\partial}{\partial\rho} \iint_{A_{\rm mix}(\rho)} F_\rho^{(z)} \, dA, \tag{8}$$

where in the last step we approximated the diapycnal density flux with its vertical component, a good approximation everywhere except in the thin BBL, which does not significantly affect the integral. This equation states that whether the near-boundary mixing transforms waters into lighter or heavier density classes in the net depends on the rate of change with density of the integral of the density flux over the part of the isopycnal experiencing mixing, not the rate of change with density of individual mixing profiles. To make this point more explicit, we follow Klocker and McDougall (2010) and write the equation in terms of quantities averaged over the near-boundary area $A_{\rm mix}$ where mixing is strong:

$$\langle\tilde{e}\rangle \simeq -\frac{\partial\langle F_\rho^{(z)}\rangle}{\partial\rho} - \langle F_\rho^{(z)}\rangle \frac{1}{A_{\rm mix}} \frac{\partial A_{\rm mix}}{\partial\rho}, \tag{9}$$

where $\tilde{e}$ is the magnitude of the diapycnal velocity, taken to be vertical and positive upward in the stratified ocean interior. The angle brackets represent the area-averaging operator $\langle\cdot\rangle \equiv A_{\rm mix}^{-1}\iint_{A_{\rm mix}} \cdot\, dA$. A positive $\langle\tilde{e}\rangle$ means that waters, on average, rise toward lighter density classes. A decrease toward the bottom of the area experiencing strong mixing, $\partial A_{\rm mix}/\partial\rho < 0$, drives diapycnal rising of dense waters, as we argued with the simple schematic in Fig. 1b.

Equation (9) differs in one very important aspect from that derived in Klocker and McDougall (2010). Klocker and McDougall (2010) took the average over the whole isopycnal layer and thus their equation had the full isopycnal area $A(\rho)$ on the right-hand side. Observing that isopycnals are nearly flat in the stratified ocean, they concluded that it is the increase in the area of the ocean basins with depth (the hypsometry) that makes $\langle\tilde{e}\rangle > 0$ and allows waters to rise across density surfaces, in spite

of mixing profiles that increase toward the bottom. Our derivation shows that the sign of $\langle \tilde{e} \rangle$ depends on the rate of change of $A_{\rm mix}$, that is, the part of the isopycnal surface experiencing strong mixing and not the rate of change of the full hypsometry.

The difference between the full A and $A_{\rm mix}$ is very important in estimating the sign of the net diapycnal transport. The area $A_{\rm mix}$ corresponds to a narrow strip annulus along the ocean boundaries, since strong mixing is confined to within a few hundred meters above the ocean bottom, as shown in Fig. 1b. If the density flux has a vertical e-folding scale d away from the bottom and the topographic slope is θ, the horizontal distance over which mixing decays by one e-folding is $d/\tan\theta$. Since isopycnal slopes are approximately flat, except for the bending within the narrow BBL, the isopycnal area experiencing strong mixing is given by the integral of $d/\tan\theta$ along the arc length where the isopycnal intersects topography, the so-called incrop line:

$$A_{\rm mix} = \alpha \int \frac{d}{\tan\theta}\, dc, \tag{10}$$

where c is the distance measured along the incrop line, and α is the number of e-folding scales after which mixing can be considered zero. Equation (10) illustrates that $A_{\rm mix}$ increases with an increase of incrop line, an increase in mixing e-folding scale, or a decrease in topographic slope. Changes of hypsometry with depth instead affect $A_{\rm mix}$ only if they are associated with lengthening or shrinking of the incrop lines.

The implication of applying Eq. (9) to $A_{\rm mix}$ rather than A is well illustrated by McDougall (1989), who studied the impact of bottom-enhanced mixing around an isolated seamount. The increase with density/depth of the circumference of a seamount implies that seamounts act as a net sink of seawater from the surrounding ocean because $\partial A_{\rm mix}/\partial\rho > 0$, even though the area of the ocean decreases downward around the seamount and $\partial A/\partial\rho < 0$. We thus expect that net diabatic upwelling is more likely near continental boundaries and ridges, where the perimeter of incrop lines increases with height above the bottom, rather than in the vicinity of seamounts.

The net diapycnal transport across the area $A_{\rm mix}$ is composed of diapycnal upwelling along the BBL and diapycnal sinking in the SML. One could use Walin's (1982) approach to estimate both components independently, and we pursue this approach in McDougall and Ferrari (2016, manuscript submitted to *J. Phys. Oceanogr.*). In this study we will estimate the BBL diapycnal transport by taking the isopycnal integral of the diapycnal velocity along the portion $A_{\rm BBL}$ of the isopycnal surface within the BBL:

$$\mathcal{E}_{\rm BBL}(\rho) = -\iint_{A_{\rm BBL}(\rho)} \tilde{\mathbf{e}} \cdot \mathbf{n}_\rho \, dA = \iint_{A_{\rm BBL}(\rho)} \frac{\nabla \cdot \mathbf{F}_\rho}{|\nabla\rho|} dA. \tag{11}$$

This integral is positive because the vertical divergence of the density flux is positive in the BBL. The SML transport $\mathcal{E}_{\rm SML}$ can be computed analogously by restricting the integral to the portion of the isopycnal in the SML, and it is negative because the flux divergence has the opposite sign there [see Eq. (4)].

The flow induced by mixing at a sloping boundary in a stratified fluid has a long history dating back to Wunsch (1970), Thorpe (1982), and Garrett (1990). These studies concentrated on mixing induced by a source of energy at the boundary, and the major focus was whether the energy was spent "mixing mixed fluid" or whether some of the boundary-generated energy was spent mixing stratified fluid above the BBL, where it is more effective in causing along-boundary diffusion and advection (Garrett 1990). By contrast, our present study assumes knowledge of the strength of mixing in the stratified fluid above the BBL. The density budget and the advection of fluid in the BBL is a slave to the flux of density it receives at its upper boundary. The difference in approach is motivated by the evidence, accumulated in the last 20 years, that topographically generated internal waves drive a mixing profile that increases toward the ocean bottom in the stratified interior above the BBL. The circulation driven by mixing is not confined to the BBL.

While the tendency for mixing to drive along-boundary flows has long been recognized, the implications for the overall ocean circulation have not. Our claim is that deep waters are transformed into denser waters by the bottom-enhanced mixing in the stratified ocean interior above rough topography and sink toward the BBLs. Once in the BBLs, the waters are transformed back to lighter waters and rise toward the surface along the ocean boundaries. In this picture, it is crucial that the boundaries are sloping because otherwise the diabatic boundary flow cannot bring waters back toward the surface. This view is quite different from the traditional explanation that ocean mixing away from boundaries drives the rise of abyssal waters through the water column. We are proposing that abyssal waters rise in the net despite the action of interior ocean mixing that, by itself, causes diapycnal downwelling.

3. Numerical model setup

Given the dearth of deep mixing measurements in the global ocean, we turn to idealized numerical simulations

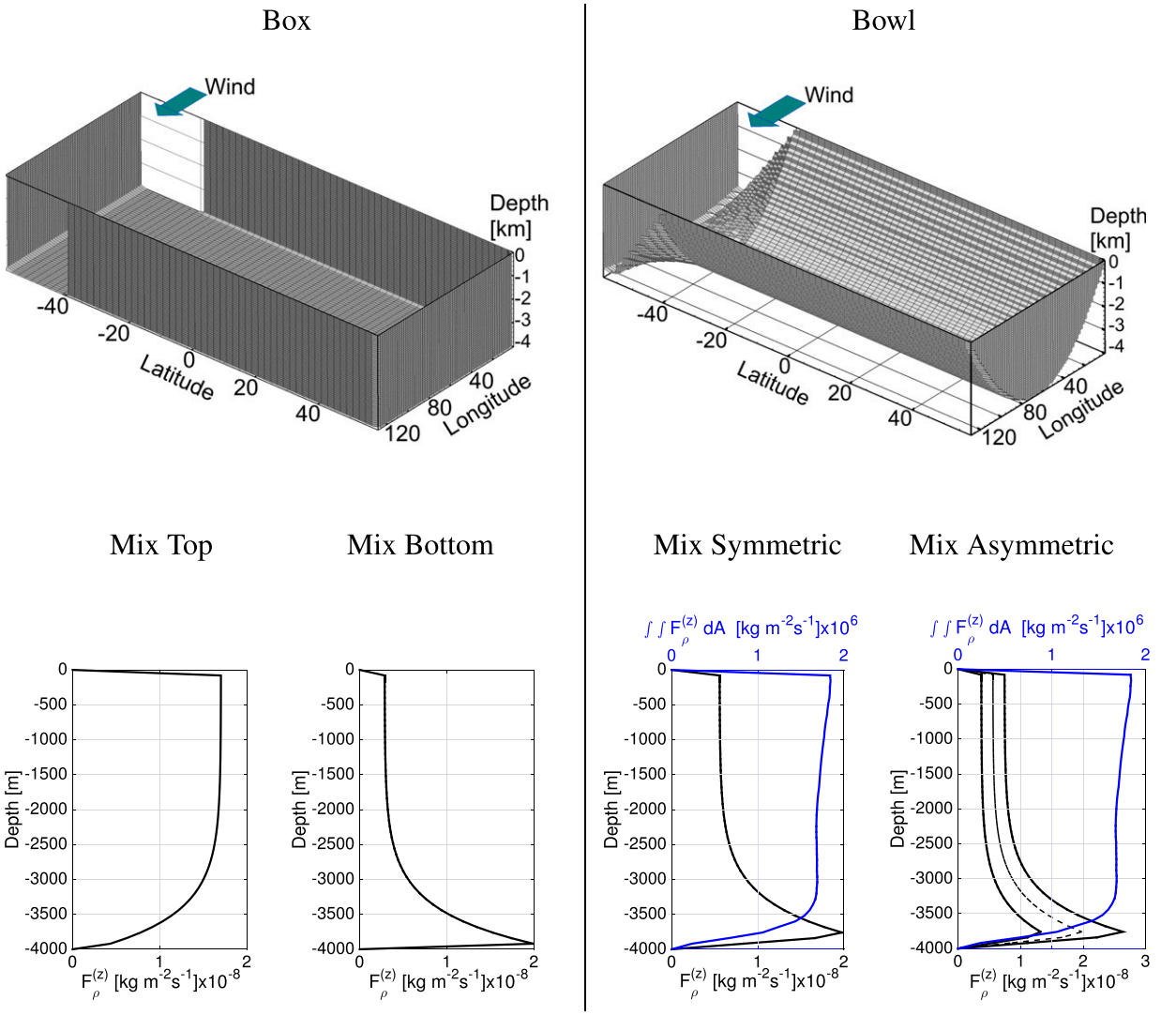

FIG. 3. (top) Model topography for the Box and Bowl simulations. (bottom) Turbulent density flux profiles $F_\rho^{(z)}$ used in the (left) Box simulations and the (right) Bowl simulations. The black lines show the density fluxes (kg m^{-2} s^{-1}) in the center of the basin for (bottom left) the Box-MixTop and (bottom center left) Box-MixBottom simulations and for the (bottom center right) Bowl-MixSymmetric and Bowl-MixAsymmetric (bottom right), while the blue lines show the area-integrated density fluxes (kg s^{-1}). For the Bowl-MixAsymmetric simulation, we show the density fluxes one grid point to the left (western half) and one grid point to the right (eastern half) of the center of the domain.

to test our claim that BBLs are key pathways for returning abyssal waters to the surface. We use the Massachusetts Institute of Technology General Circulation Model (MITgcm; Marshall et al. 1997) in two different configurations sketched in the top panels of Fig. 3. Both configurations include a single basin bounded by walls to the north, east, and west and connected to a reentrant channel to the south. The Box configuration has a flat bottom 4000 m deep, as shown in Fig. 3 (top left), while the Bowl configuration consists of a bowl-shaped basin and a flat-bottom, 4000-m-deep channel, as shown in Fig. 3 (top right) (the deepest point in the center of the basin reaches 4000 m). The model vertical resolution is uniform and equal to 80 m. The horizontal resolution is 2° × 2°. The domain at the surface extends over 130° of longitude and from 60°S to 60°N for a total basin surface area approximately equal to that of the Pacific Ocean. There are no lateral boundaries between 60° and 40°S, and the flow in this range is zonally periodic. This setup is best thought of as an idealization of the circulation in a closed basin, like the Pacific Ocean, connected to a laterally unbounded channel to the south, like the Southern Ocean.

The model is forced at the surface by restoring temperature to a prescribed profile on a time scale of a month over the 80-m-thick topmost grid cell. The

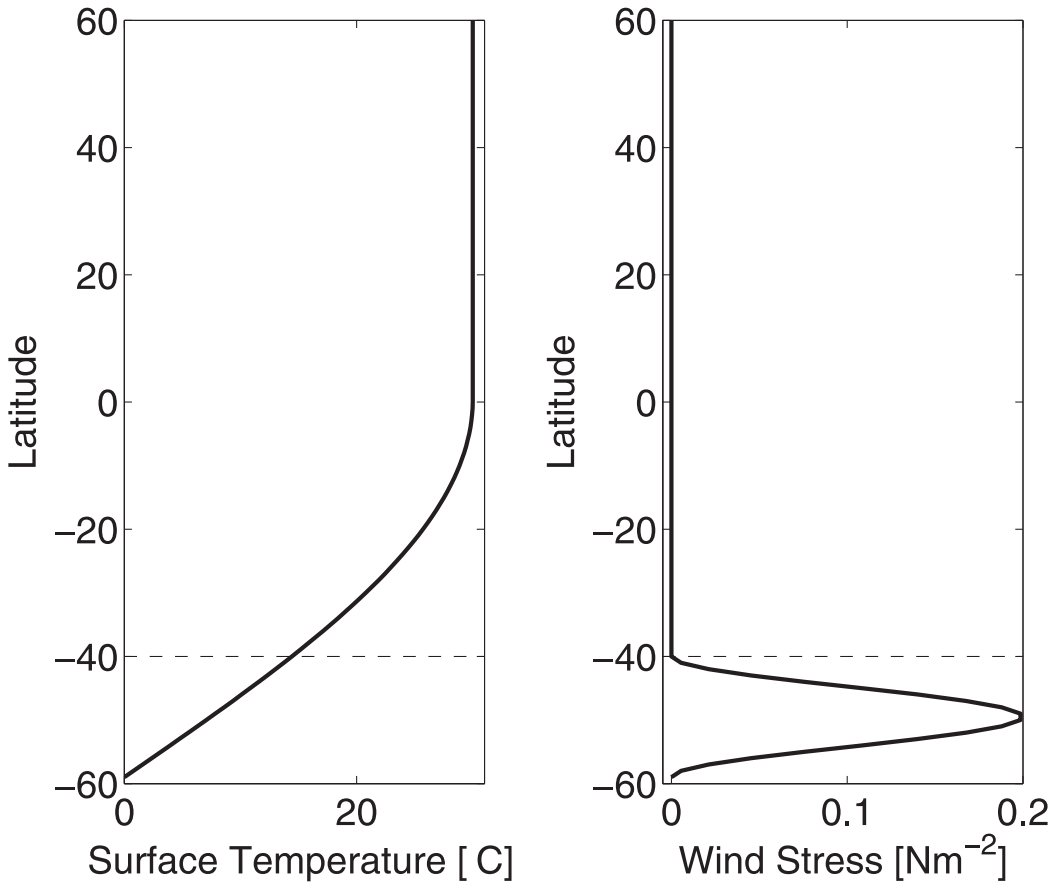

FIG. 4. (left) The air temperature profile to which the ocean surface temperature is restored and (right) the wind stress profile applied at the ocean surface for all the simulations described in the paper.

restoring temperature profile, shown in the left panel of Fig. 4, increases monotonically with latitude from the southern boundary to the equator and then remains constant; the profile is constant in the zonal direction. We use a linear equation of state and set salinity to a constant; thus, density is only a function of temperature and equal to $\rho = \rho_0[1 - \alpha(T - T_0)]$, where $\rho_0 = 1035\,\mathrm{kg\,m^{-3}}$, $T_0 = 6.5°\mathrm{C}$, and $\alpha = 2 \times 10^{-4}\,°\mathrm{C}^{-1}$. The restoring temperature profile is chosen to drive convection and formation of dense waters at the southern edge of the channel but not in the Northern Hemisphere, like in today's North Pacific Ocean. A zonally uniform wind stress, shown in the right panel of Fig. 4, blows only over the channel; the stress peaks at $0.2\,\mathrm{N\,m^{-2}}$ in the center of the channel and decays toward its northern and southern edges. We do not impose a wind stress over the basin to avoid spinning wind-driven gyres of no relevance to the deep stratification and circulation investigated here. Similar model setups have been employed in the literature to study the ocean overturning circulation (e.g., Nikurashin and Vallis 2011; Wolfe and Cessi 2011; Munday et al. 2013; Mashayek et al. 2015).

A number of processes need to be parameterized because they arise at scales not resolved by the model grid. The slumping of density surfaces by baroclinic instability is parameterized with the Gent and McWilliams (1990) scheme with a lateral diffusivity of $1000\,\mathrm{m^2\,s^{-1}}$. We do not prescribe any background along-isopycnal diffusivity because our only tracer is temperature and does not have any gradients along temperature/density surfaces. Turbulent momentum fluxes are parameterized with horizontal and vertical viscosities of $\nu_H = 2 \times 10^5\,\mathrm{m^2\,s^{-1}}$ and $\nu_V = 1.2 \times 10^{-4}\,\mathrm{m^2\,s^{-1}}$, respectively, and a linear bottom drag with a drag coefficient of $5 \times 10^{-4}\,\mathrm{m\,s^{-1}}$.

Representation of vertical mixing of density

Our goal is to study how the bottom intensification of mixing influences the overturning circulation and stratification in idealized channel plus basin simulations. The traditional approach is to parameterize turbulent mixing through a vertical turbulent diffusivity, based on an analogy with molecular mixing. However, this approach does not constrain the vertical profile of the turbulent density flux,

which is the product of the turbulent diffusivity times the density stratification. Alternatively, we prescribe the turbulent density flux itself $F^{(z)}_{\rm mix}$ as a forcing on the right-hand side of the density (technically temperature) equation:

$$\frac{D\rho}{Dt} = -\frac{\partial F^{(z)}_{\rm mix}}{\partial z}. \tag{12}$$

Oka and Niwa (2013) followed a similar approach to represent deep mixing in simulations of the Pacific Ocean, where they prescribed a turbulent density flux based on an estimate of mixing induced by breaking internal tides.

Our choice of imposing the turbulent density flux should not be read as implying that the profile of mixing is independent of stratification; for example, mixing ought to vanish in the absence of stratification. We impose the turbulent density flux because our goal is to diagnose what circulation and stratification are consistent with a particular mixing profile rather than to simulate the interactions between the large-scale ocean structure and the small-scale turbulent mixing. To the extent that the solution is characterized by a stratified abyss and a strong overturning circulation that crosses density surfaces, we will conclude that the solution is qualitatively consistent with the observed present-day ocean. Otherwise, we will conclude that the turbulent density flux profile is not consistent with what we know about the abyssal ocean. Anticipating our results, we will find that bottom-intensified mixing is consistent with the observed abyssal ocean only if the ocean basin has sloping lateral walls, but not if it has vertical walls.

We will consider four simulations with different mixing and topography profiles. Two Box simulations have vertical sidewalls and mixing profiles that either decrease or increase above the BBL (and go to zero within the BBL), as shown in the two left panels at the bottom of Fig. 3. Two Bowl simulations have sloping sidewalls and mixing profiles that decrease with height above the BBL (before going to zero in the BBL) but such that the area-integrated mixing profile increases with height z. One Bowl simulation uses the same mixing profile everywhere, while the other has a larger mixing on the eastern half of the domain, so as to mimic a situation with nonhomogeneous mixing. The topographic shapes and the corresponding mixing profiles are shown in Fig. 3.

Our approach of prescribing a nonmonotonic turbulent density flux can lead to unstable stratification. Surface cooling can also lead to unstable density profiles. In the real ocean, convection develops when the density stratification is unstable. In our hydrostatic model, convection is parameterized by locally increasing the turbulent diffusivity (which is otherwise zero) until the stratification is once again stable. This parameterization results in an additional turbulent density flux $F^{(z)}_{\rm conv}$. The total turbulent density flux is therefore given by

$$F^{(z)}_{\rho} = F^{(z)}_{\rm mix} + F^{(z)}_{\rm conv}. \tag{13}$$

In the simulations described below, the convective contribution leads to a small quantitative change and no qualitative change to the prescribed turbulent density flux, and $\partial F^{(z)}_{\rho}/\partial z$ has the same sign as $\partial F^{(z)}_{\rm mix}/\partial z$.

While we do not prescribe a vertical turbulent diffusivity, we can infer the vertical turbulent diffusivity from our solutions through

$$\kappa \equiv -\frac{F^{(z)}_{\rho}}{\partial_z \rho}. \tag{14}$$

Our numerical study can therefore be interpreted as a diagnostic calculation to find the turbulent diffusivity profile that is necessary to obtain a turbulent density flux profile consistent with observations.

4. Numerical model results

In all simulations the zonally averaged circulation in the southern channel is the result of two opposing forces. The eastward winds drive a thermally indirect overturning circulation, that is, a circulation with dense waters rising at the southern edge of the channel and light waters sinking at its northern edge. The parameterized baroclinic eddies drive an opposing thermally direct circulation with dense waters sinking at the southern edge of the channel and light waters rising at its northern edge (Marshall and Radko 2003). In our setup, the thermally direct circulation dominates because the surface cooling at the southern edge of the channel weakens the vertical stratification by driving upright convection to the ocean bottom (the analog of dense water formation in the Southern Ocean.). In weakly stratified waters, the slumping of isopycnals by baroclinic instability is very rapid and generates a very strong eddy-driven overturning circulation. In all our simulations the overturning circulation is thermally direct with abyssal waters sinking in the channel and rising toward the surface in the closed basin, regardless of the mixing profile. Nikurashin and Vallis (2011) pointed out that without mixing in the ocean basin, this circulation would be confined to the Southern Ocean. Mixing in the basin is crucial in connecting the overturning circulation and stratification between the channel and the basin.

In this section, we illustrate how the overall solution changes for different profiles of vertical mixing. In sections 4a and 4b, we show that in an ocean with a flat-bottom topography, a deep stratification can be maintained only if

the turbulent density flux increases toward the surface, contrary to what is observed in the abyssal ocean. Section 4c shows that, if the boundaries are sloped, a deep stratification can be maintained with a turbulent density flux that decreases with height above the BBL. This stable stratification can exist in steady state because waters upwell toward the surface along the sloping boundaries, where the turbulent density flux divergence is positive. Section 4d explores the effect of variations in the profile of mixing along the sloping topography.

a. *Box simulation with a turbulent density flux profile increasing above the BBL*

In this first Box-MixTop experiment, we consider an ocean with a flat bottom, vertical sidewalls, and a turbulent density flux profile that starts from zero at the ocean bottom and increases toward the surface before dropping back to zero over the topmost grid cell (see Fig. 3). This is a scenario where the turbulent density flux divergence generated by mixing in the ocean interior is positive, unlike in the present ocean, and thus waters are expected to rise from the abyss toward the surface everywhere in the basin.

In the topmost grid cell, the turbulent density flux is set through restoring to the atmospheric temperature in Fig. 4 and results in surface cooling. Below the surface, starting at $z = -80\,\mathrm{m}$, a turbulent density flux is prescribed according to the formula

$$F^{(z)}_{\mathrm{mix}} = (F_b - F_t)[1 - e^{-(z+H)/d}], \tag{15}$$

where H is the ocean depth set to 4000 m, and d is the 500-m e-folding scale over which the mixing profile increases from 0 at the bottom to $(F_b - F_t)$ at $z = -80\,\mathrm{m}$. The parameters F_t and F_b are representative values of the top and bottom density fluxes generated by breaking waves in the global ocean. The estimates are based on a 3D map of kinetic energy dissipation due to breaking waves published by Nikurashin and Ferrari (2013). Following Osborn's (1980) argument that only 20% of the dissipated energy contributes to mixing, they estimated that the turbulent density flux along the ocean bottom is $F_b = 2.0 \times 10^{-8}\,\mathrm{kg\,m^{-2}\,s^{-1}}$, and 4000 m above the bottom it is $F_t = 0.2 \times 10^{-8}\,\mathrm{kg\,m^{-2}\,s^{-1}}$ (equivalent to buoyancy fluxes of $2.0 \times 10^{-10}\,\mathrm{m^2\,s^{-3}}$ and $0.2 \times 10^{-10}\,\mathrm{m^2\,s^{-3}}$, respectively). In this first simulation, we turn the mixing profile upside down and set the top value at $z = -80\,\mathrm{m}$ equal to $F_b - F_t \approx F_b$. The resulting turbulent density flux profile is plotted in the MixTop panel of Fig. 3.

The top-left panel of Fig. 5 confirms that the zonally averaged circulation in this simulation is thermally direct: waters flow southward at the surface in the channel, consistent with surface cooling, sink into the abyss at the southern edge of the channel, and then rise back in the closed ocean basin. The overturning circulation is calculated as the meridional mass transport below a density level ρ:

$$\Psi(y,\rho) = \overline{\int_{\rho' \le \rho} [v(x,y,z,t) + v_{\mathrm{GM}}(x,y,z,t)]\,dx}, \tag{16}$$

where v is the meridional velocity, and v_{GM} is the meridional velocity induced by the Gent and McWilliams (1990) parameterization of ocean eddies generated through baroclinic instability. The overbar denotes a time average taken over 10 years, after the model has reached equilibrium, to remove any time dependence. The overturning is then plotted in (y, z) space, with z the average depth of the isopycnal ρ. This definition is often referred to as the residual overturning circulation (Nurser and Lee 2004) because it includes both the transport by the zonally averaged meridional velocity and the opposing eddy transport associated with parameterized eddies and fluctuations of the isopycnal ρ. The residual overturning is the most appropriate diagnostic of the overturning because it describes the pathway followed by waters in latitude–depth space.

The rising of waters from the abyss in the closed ocean basin is confirmed in the middle-left panel of Fig. 5, where we show representative longitude–depth sections in the basin of the diapycnal velocity $\tilde{\mathbf{e}}$ induced by the full turbulent density flux $F^{(z)}_{\rho} = F^{(z)}_{\mathrm{mix}} + F^{(z)}_{\mathrm{conv}}$ [Eq. (13)]. The diapycnal velocity is everywhere upward because $\partial F^{(z)}_{\rho}/\partial z > 0$ and the contribution of horizontal fluxes to the full divergence is negligible [see Eq. (4)].

The bottom-left panel of Fig. 5 shows the rate at which waters cross a particular isopycnal in the ocean interior [Sverdrups (Sv); $1\,\mathrm{Sv} \equiv 10^6\,\mathrm{m^3\,s^{-1}}$], that is, the diapycnal velocity averaged over time and integrated along the near-boundary portion of the isopycnal experiencing mixing as per Eq. (8). (In practice, we verified that it is sufficient to stop the area integrals a few grid points below the surface to guarantee that we capture transports driven by interior mixing and not by air–sea fluxes.) The black bars represent the net diapycnal transport $\mathcal{E}$, which is equal to the difference of the red bars, representing the total diapycnal upwelling in the BBL, $\mathcal{E}_{\mathrm{BBL}}$ in Eq. (11), and the blue bars represent the total diapycnal sinking in the stratified interior $\mathcal{E}_{\mathrm{SML}}$. These diapycnal transports are often referred to as transformation rates in oceanography, and we will use diapycnal transport and transformation rates interchangeably. The net transport is everywhere positive, implying that both interior and BBL mixing transform deep waters into light ones, consistent with the imposed turbulent density flux (convection has little effect on the calculation in this simulation):

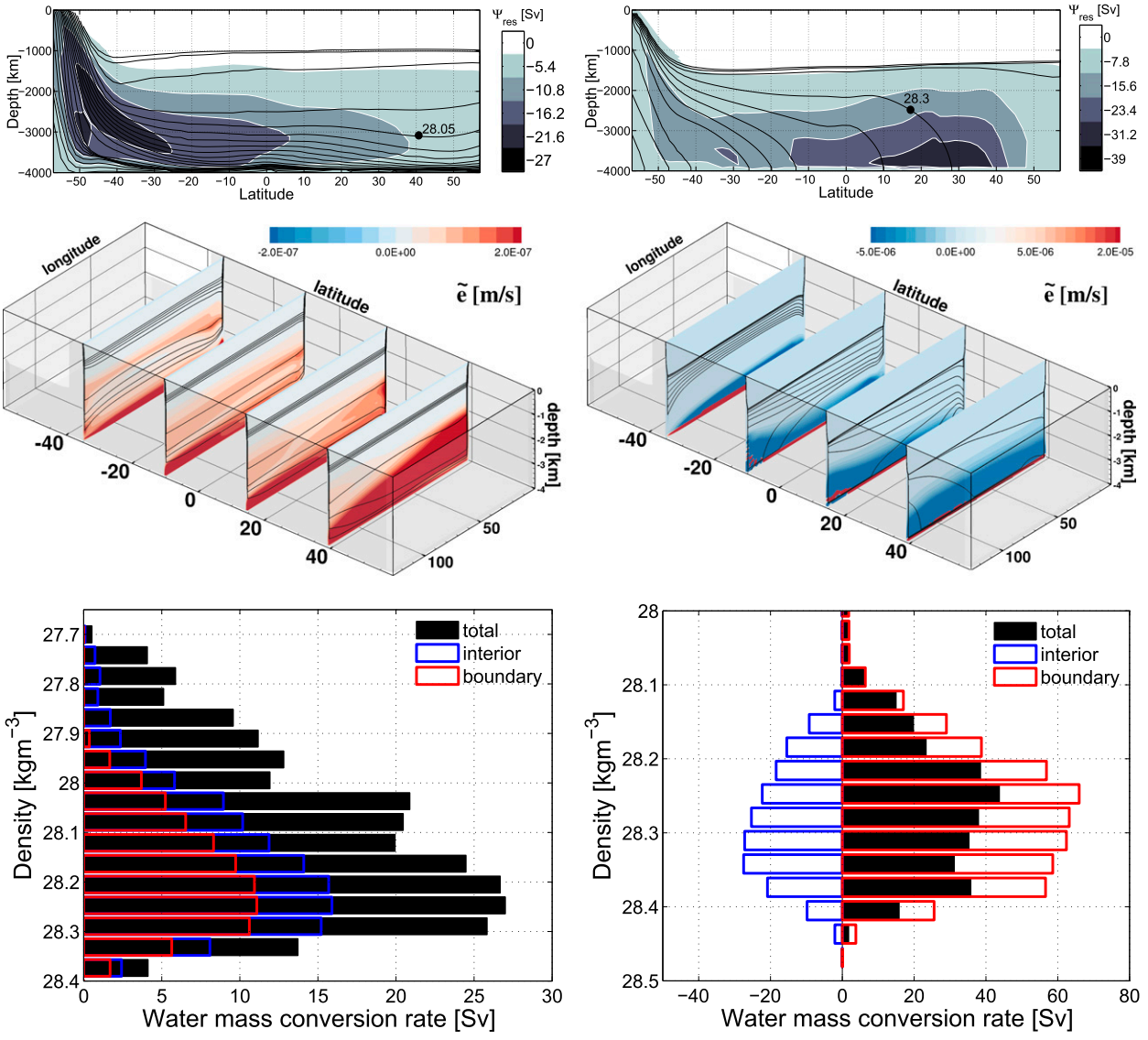

FIG. 5. (left) Results from the Box-MixTop simulation with vertical sidewalls and a turbulent density flux profile increasing toward the ocean surface and shown in the MixTop panel of Fig. 3. The top panel shows the residual overturning streamfunction in Sv calculated using Eq. (16) (gray shading) and sample isopycnals spaced by 0.025 kg m^{-3} at depths where there is substantial overturning (black lines). The middle panel shows the diapycnal velocity, along four longitude–depth sections in the basin, computed using Eq. (4). The diapycnal velocities in the basin are everywhere positive and reach 4×10^{-7} m s^{-1}. The black lines are isopycnal contours spaced by 0.1 kg m^{-3}. The bottom panel shows the water mass transformations (Sv) computed with Eq. (6) for the portion of the isopycnal surface in the ocean interior above the BBL (blue bars) in the BBL (red bars) and for the sum of the two contributions (black bars). (right) Results from the Box-MixBottom simulation with vertical sidewalls and a turbulent density flux profile decreasing toward the ocean surface and shown in the Mix-Bottom panel of Fig. 3. The panels in the right column show the same diagnostics as in the left column. In this simulation the diapycnal velocities are positive in the BBL with values reaching 3×10^{-5} m s^{-1} and negative in the ocean interior with values reaching only -1×10^{-6} m s^{-1}.

$$\frac{D\rho}{Dt} = -\frac{\partial F_\rho^{(z)}}{\partial z} < 0. \tag{17}$$

The top-left panel of Fig. 5 shows that the stratification consists of steeply sloped isopycnals (black contours) in the channel and nearly horizontal isopycnals in the basin. The isopycnal slope in the channel is set through a balance between the wind stress and the eddy-driven circulation (e.g., Marshall and Radko 2003; Nikurashin and Vallis 2011). The stratification in the basin is instead maintained through a balance between the advection of density by the residual overturning and vertical diffusion of density driven by mixing, consistent with Munk's (1966) "abyssal recipes"

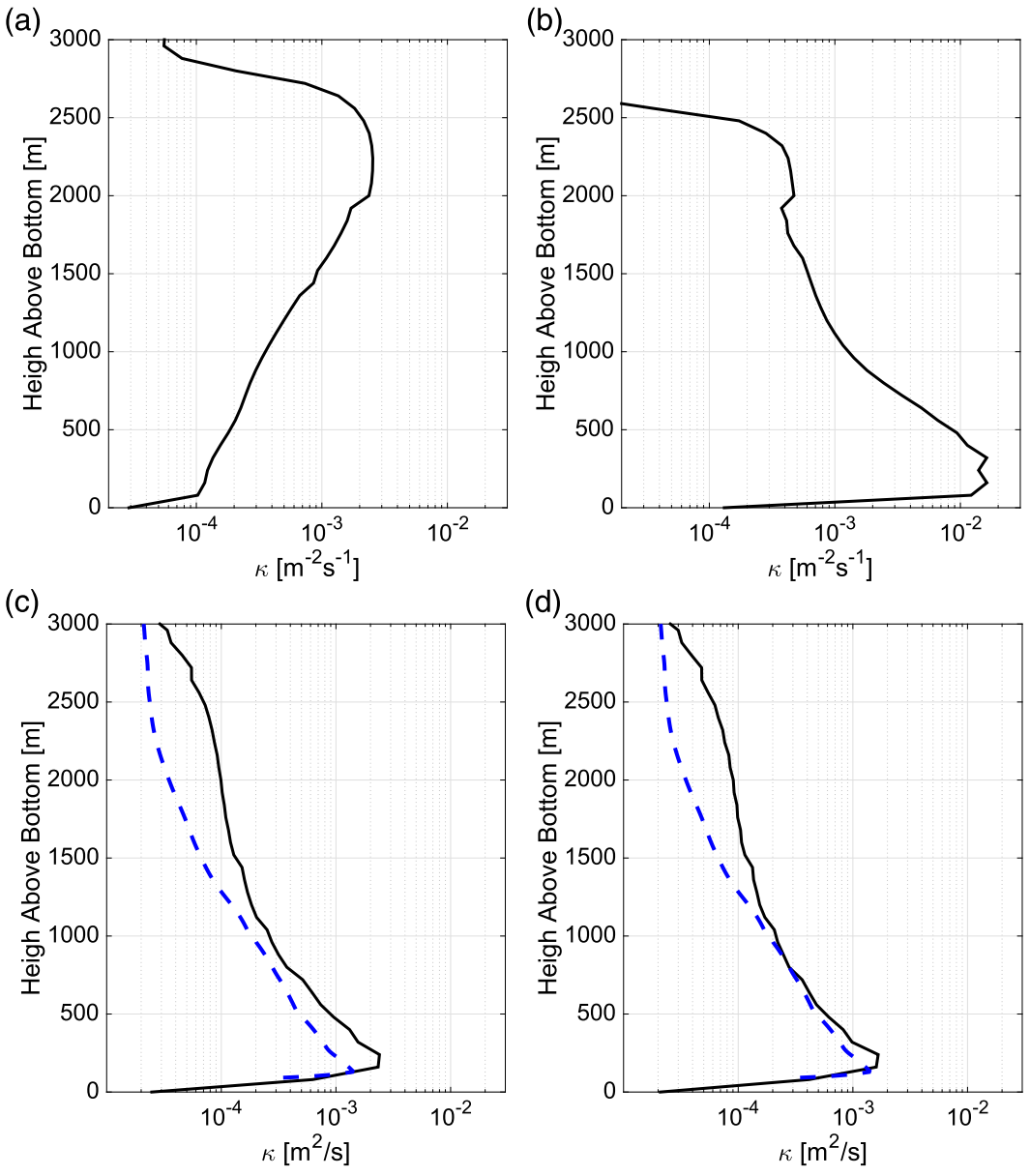

FIG. 6. Diapycnal turbulent diffusivities computed with Eq. (14) based on the turbulent density fluxes and the stratification obtained in the various simulations (solid lines). The diapycnal diffusivity based on the turbulent density flux and stratification for the Pacific Ocean based on the calculation described in Nikurashin and Ferrari (2013) (dashed lines). (a) Box simulation with a turbulent density flux increasing above the BBL. (b) Box simulation with a turbulent density flux profile decreasing above the BBL. (c) Bowl simulation with a turbulent density flux profile decreasing above the BBL with the same bottom value everywhere. (d) Bowl simulation with a density flux profile decreasing everywhere above the BBL, but twice as large in the eastern half of the domain than in the western half.

hypothesis. In the upper ocean, the stratification becomes very large because the turbulent density flux is balanced by a weak advection (not shown). In the real ocean, this does not happen because shallow waters are ventilated by wind forcing and Northern Hemisphere convection, while turbulent mixing becomes second order.

The turbulent diffusivity implied by the stratification and turbulent density flux obtained from the simulation at equilibrium is calculated using Eq. (14). Its horizontal average over the basin is shown in Fig. 6a. The turbulent diffusivity increases from $\sim 1 \times 10^{-4}\,\mathrm{m^2\,s^{-1}}$ at the ocean bottom to $\sim 2 \times 10^{-3}\,\mathrm{m^2\,s^{-1}}$ at 2000-m depth. (The sudden decrease of κ in the BBL reflects the vanishing of

the turbulent density flux there.) A turbulent diffusivity that increases with height above the ocean bottom is not consistent with observations.

The take home message is that this simulation with vertical sidewalls resulted in an overturning circulation and stratification broadly consistent with those observed in the abyssal Pacific Ocean, but it required a turbulent density flux divergence and a vertical profile of turbulent diffusivity opposite to the ones observed in the abyssal ocean. Can one obtain a similar circulation and stratification for a realistic turbulent density flux profile?

b. *Box simulation with a turbulent density flux profile decreasing above the BBL*

In the Box-MixBottom simulation, the prescribed turbulent density flux between $-80 < z < -3920\,\mathrm{m}$ decreases with height according to the formula

$$F_{\mathrm{mix}}^{(z)} = F_t + (F_b - F_t)e^{-(z+H)/d}, \tag{18}$$

with the same parameter values given in the previous section. The turbulent density flux goes linearly to zero at the ocean bottom over an 80-m-thick BBL and at the ocean surface over an 80-m-thick surface mixed layer (i.e., one grid point in the vertical). The profile is shown in the MixBottom panel of Fig. 3. The surface density flux at the topmost grid cell is set through restoring to the same atmospheric temperature profile used for all simulations. The bottom topography is flat, and the lateral sidewalls are vertical.

Naively one might guess that this mixing profile ought to drive downwelling in the basin, resulting in a thermally indirect overturning circulation with cold waters upwelling along the southern edge of the channel and then flowing toward the basin to sink back into the abyss. However, a thermally indirect overturning circulation is inconsistent with the air–sea cooling applied over the channel. Indeed the overturning circulation diagnosed from the simulation and shown in the top-right panel of Fig. 5 is thermally direct with cold waters sinking along the southern edge of the channel and rising nearly adiabatically along the steep isopycnals in the basin. Contrary to the naive inference, the overturning is thermally direct, but the deep ocean is very weakly stratified, unlike in the Box-MixTop simulation.

To gain insight in this simulation, it is useful to draw an analogy with the tropical atmosphere. The prescribed mixing profile drives an increase in temperature (and hence a decrease in density) over the bottom grid cell and cooling (an increase in density) in the rest of the water column, much like the radiative budget of the atmosphere, which is characterized by warming at the sea–land surface and radiative cooling above. As observed in the tropical atmosphere, the bottom heating triggers upright convection and pretty much erases any vertical stratification in the basin (ocean eddies in the basin are too weak to maintain a stratification, like eddies in the tropical atmosphere and unlike eddies in the extratropical atmosphere). The model output confirms that convective adjustment is active below 1500 m, where the stratification is weak. The thickness of this unstratified abyssal layer depends on the particular profile of vertical mixing and the value of the air–sea density flux, which is weak and negative along most of the basin.

While the vertical stratification in the bottom convective layer is weak, there is a substantial horizontal stratification. The waters flow northward along the BBL, where the turbulent density flux divergence is positive and allows a flow toward lighter density classes. The middle-right panel of Fig. 5 confirms that the diapycnal velocity is positive along the BBL as waters flow horizontally and cross the isopycnals that intersect the ocean bottom; the diapycnal upwelling in the BBL is horizontal in the absence of sloping boundaries. The waters then flow back toward the channel approximately along the curved isopycnals, but at a somewhat smaller slope, as they gain density through the imposed negative turbulent density flux divergence. The middle-right panel of Fig. 5 confirms that the diapycnal velocity is negative in the interior and much weaker in magnitude than in the BBL.

The bottom-right panel of Fig. 5 shows that waters are transformed to lighter density classes in the net, but this transformation is the result of a large cancellation between the transformation into lighter density classes within the BBL, where $\nabla \cdot \mathbf{F}_\rho > 0$, and an opposite transformation into heavier density classes in the interior, where $\partial F_\rho^{(z)}/\partial z < 0$. The net transformation must be positive to balance the surface cooling, and this is achieved by adjusting the isopycnals so that they all bend downward and intersect the BBL, where mixing converts the dense waters formed at the channel surface back to lighter waters. The naive thinking that mixing dictates whether waters rise or sink fails to recognize that the geometry of isopycnals can also be modified by the mixing profile.

The solution with hardly any abyssal stratification depicted in the right column of Fig. 5 is very different from that observed in the deep oceans. An ocean with vertical sidewalls and a realistic turbulent density flux profile results in a stratification not consistent with observations. This solution is also somewhat physically inconsistent. Mixing is generated by breaking internal waves. In the limit of weak stratification, as

obtained in the simulation, the internal wave field would vanish together with the associated mixing.

Figure 6b shows the turbulent diffusivity calculated from Eq. (14) and averaged horizontally over the whole basin. A very large diffusivity κ, increasing beyond 10^{-2} $m^2 s^{-1}$ at the ocean bottom, is required to drive a bottom-intensified turbulent density flux with a traditional diffusive closure: $F_\rho^{(z)} = -\kappa \partial_z \rho$. The inescapable conclusion is that a flat-bottom channel plus basin simulation with a turbulent density flux profile decreasing upward does not result in an ocean with deep stratification and a thermally direct overturning circulation. A similar conclusion was reached by Mashayek et al. (2015) and casts doubt on idealized models of the abyssal overturning circulation that use a flat bottom and a prescribed turbulent diffusivity (e.g., Nikurashin and Vallis 2011; Munday et al. 2013; Mashayek et al. 2015). To the extent that such models are used to study the impact of mixing on the deep circulation, they fail to reproduce the bottom enhancement of the turbulent density flux profile observed in the abyssal ocean.

c. *Bowl simulations with a turbulent density flux profile decreasing above the BBL*

The two simulations with a sloping topography better capture the stratification and overturning circulation observed in the deep ocean. In the Bowl simulations the topography in the basin has a parabolic shape. The topography is instead flat in the channel as shown in the top-right panel of Fig. 3. First, we consider a simulation where the prescribed turbulent density flux in the interior, above the BBL, decreases with height above the bottom according to the formula

$$F_\rho^{(z)} = F_t + (F_b - F_t) e^{-(z+H)/d}, \tag{19}$$

where H is the local depth that varies with longitude in the bowl, z is depth, d is 500 m, and the flux parameters are $F_b = 2.0 \times 10^{-8}\,\mathrm{kg\,m^2\,s^{-1}}$ and $F_t = 1.0 \times 10^{-8}\,\mathrm{kg\,m^2\,s^{-1}}$. The flux goes linearly to zero over the last two grid points for a 160-m-thick BBL, as shown in the Mix Symmetric panel of Fig. 3. We run simulations where the BBL was only 80 m thick, as in the Box simulations, and found identical results to the ones presented here, but the diagnostics of diapycnal velocities in the BBL were much noisier.

The shape of the topography and the value of turbulent density flux divergence are chosen such that the turbulent density flux profile integrated over the full basin area at fixed depth increases toward the surface, even though each individual flux profile decreases with height above the BBL (both profiles are shown in the bottom panel for the Mix Symmetric simulation in Fig. 3). The value of F_t is larger than in the Box simulations to reduce by 30% the turbulent density flux divergence. With a smaller divergence, it is easier to pick a topographic shape such that the second term on the right-hand side of Eq. (9) dominates over the first, resulting in net upwelling throughout the basin. The parabolic topography has very weak slopes toward the bottom of the basin so that the whole ocean area experiences strong mixing and $A_{\mathrm{mix}} = A$ in the deepest 1 km of the bowl.[2] The area of strong mixing A_{mix} hardly increases above the bottom kilometer, unlike the full area A, because strong mixing is confined to narrow ribbons along the boundaries whose area is nearly constant with height. According to Eq. (6), it is the area experiencing mixing along an isopycnal, and not at constant depth, that sets the sign of the water mass transformation in the basins. However, isopycnals are mostly flat in the Bowl simulations, except in the thin BBLs where they bend to intersect topography at right angles. Thus, the sign of the divergence of the turbulent density flux is not very sensitive to whether the integration is taken along isobaths or isopycnals. This is also true for the estimate of the turbulent density flux for the global ocean presented in the next section.

The left column of Fig. 7 shows the results for the first Bowl simulation. Starting from the top-left panel, we see that the ocean is fully stratified at depth, despite a turbulent density flux profile that decreases toward the surface. In contrast to the Box-MixBottom simulation, no convection develops at depth. The zonally averaged overturning circulation is thermally direct with waters sinking at the southern edge of the channel and rising back toward the surface in the basin. However, the middle-left panel of Fig. 7 shows that the zonally averaged picture is somewhat misleading because the overturning is the result of waters sinking toward higher densities in the basin interior (blue diapycnal velocities) and waters rising toward lighter density classes at much faster speeds along the thin BBL (red diapycnal velocities). The bottom-left panel of the figure confirms that the interior water mass transformation into heavier density classes is overwhelmed by a larger transformation into lighter density classes along the BBLs: $\mathcal{E}_{\mathrm{BBL}} = 35$ Sv of waters flow upslope across density surfaces along the BBL and $\mathcal{E}_{\mathrm{SML}} = 20$ Sv sink diapycnally in the stratified interior. The zonally averaged overturning of approximately 15 Sv shown in the upper-left panel of Fig. 7 is the

[2] The bathymetry has small slopes in the bottom 1 km and mixing extends a distance $d/\tan\theta \sim 10$ latitude degrees away from the lateral boundaries. Thus, the area experiencing mixing increases with the basin area in the bottom kilometer.

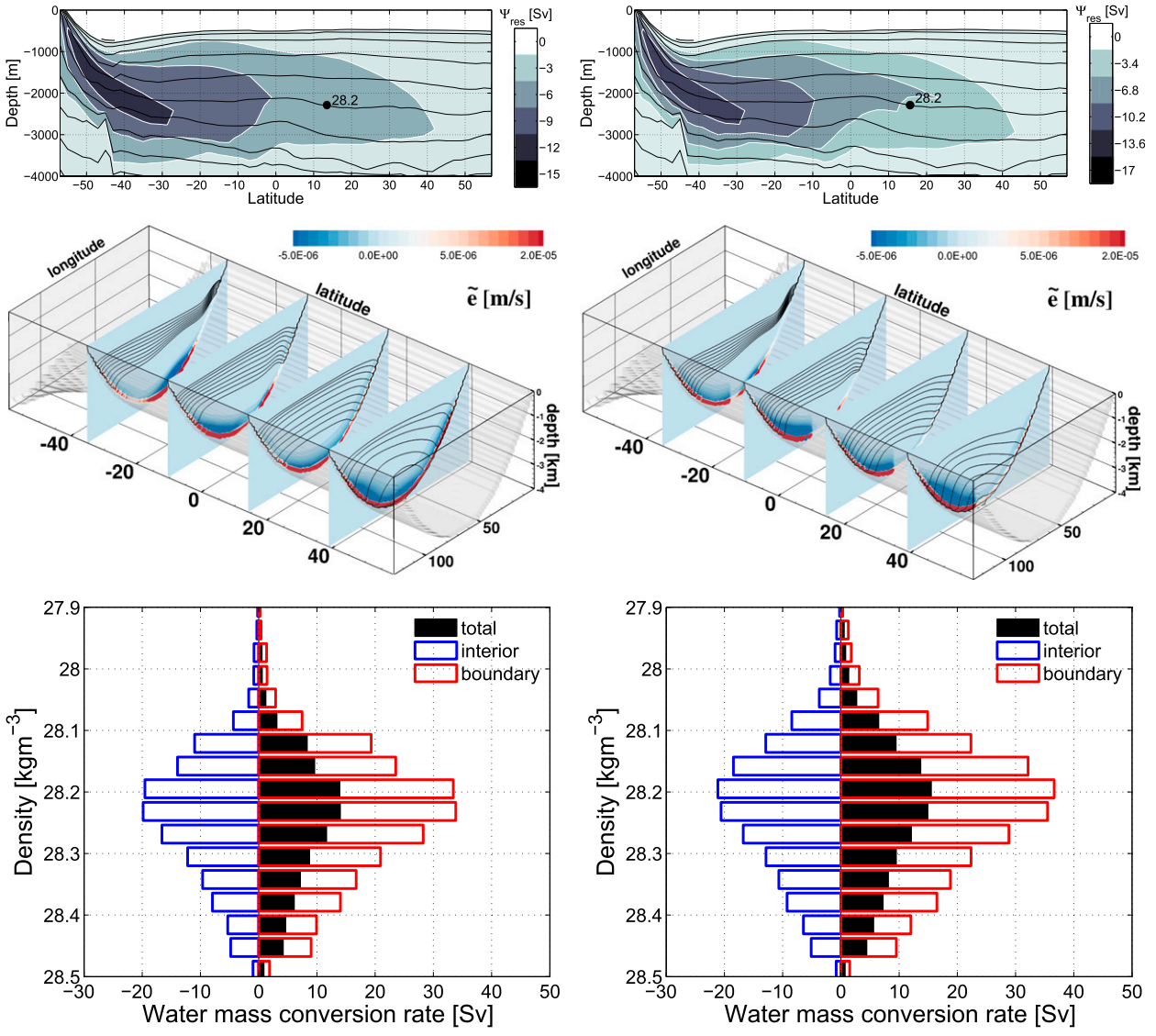

FIG. 7. (left) Results from a Bowl simulation with a turbulent density flux profile decreasing with height above the parabolic ocean bottom as shown in the Mix Symmetric panel of Fig. 3. The three panels show the overturning streamfunction, the diapycnal velocity, and the water mass transformation, respectively, as described in the caption of Fig. 5. The diapycnal velocities are positive along the BBL with values reaching 1×10^{-5} m s^{-1} and negative in the ocean interior with values reaching only -1×10^{-6} m s^{-1}. (right) Results from a Bowl simulation with a turbulent density flux profile decreasing above the bottom, but twice as large in the eastern as in the western half of the domain as shown in the Mix Asymmetric panel of Fig. 3. The three panels in the right column show the same diagnostics as in the left column. In this simulation the diapycnal velocities in the eastern half of the basin are twice as large as those in the western half.

small residual of these much larger interior and boundary transports.

This circulation pattern confirms our theoretical prediction that topography exerts a strong control on the ocean circulation. The rapid increase in the length/perimeter of isobaths with height is crucial to allow waters to upwell in the net, despite a mixing profile that decays with height above the bottom. Unexpectedly, the net overturning circulation is the residual of two much larger and opposite diapycnal transports: downwelling of waters in the ocean interior (blue bars) and upwelling of waters along the boundaries (red bars). In the next section, we will provide tantalizing evidence that this is not only the case in our idealized simulations but possibly in the abyssal ocean as well.

The importance of topography is best illustrated by comparing the Box-MixBottom and Bowl simulations. In both simulations the air–sea fluxes in the channel convert light waters into heavy ones that sink to the bottom and flow toward the basin. In the Box-MixBottom simulation

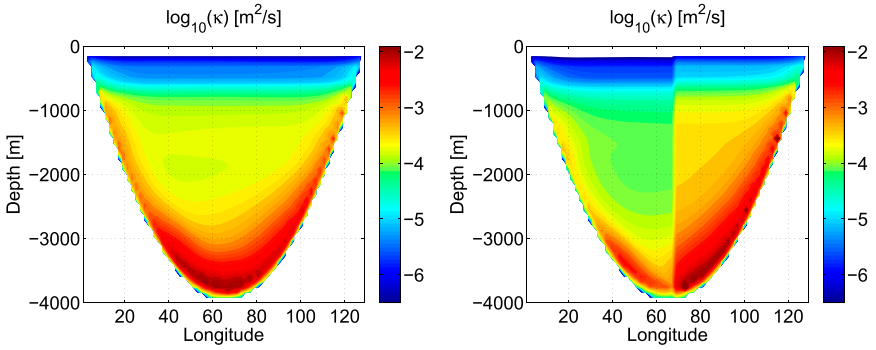

FIG. 8. Diapycnal turbulent diffusivities computed with Eq. (14) based on the turbulent density fluxes and the stratification obtained in the (left) Bowl-Symmetric and (right) Bowl-Asymmetric simulations. The diffusivities are averaged meridionally over the latitudes corresponding to the closed basin and plotted as a function of depth and longitude.

with a turbulent density flux profile decreasing toward the surface, the isopycnals in the basin bend downward to intersect the BBL at the ocean flat bottom, where waters can be converted back into lighter waters to close the overturning circulation loop. In the Bowl configuration, isopycnals in the basin are nearly flat and intersect the BBL at the lateral boundaries. The topography is crucial in allowing the ocean basin to remain stratified with a thermally direct circulation.

Figure 6c shows the basin-averaged turbulent diffusivity as a function of height above the bottom implied by the turbulent density flux and stratification in the equilibrated solution. The diffusivity peaks at $2 \times 10^{-3}\,\mathrm{m^2\,s^{-1}}$ above the BBL and decays by an order of magnitude over 1000 m. These values are consistent with the diffusivity profiles implied by the turbulent density fluxes for the abyssal ocean estimated by Nikurashin and Ferrari (2013) for the Pacific Ocean, the basin with a circulation and stratification closest to our simulations (see dashed line in Fig. 6c and next section). We also show a longitude–depth map of the turbulent diffusivity averaged over the latitudes corresponding to the closed basin in Fig. 8 (left panel). The map highlights that the largest values of κ are confined to the deepest part of the basin, where stratification is weakest, and they decrease upward.

The last simulation we consider is equivalent to the Bowl-MixSymmetric simulation we just described, except that the turbulent density flux profile is different on the eastern and western halves of the domain, as shown in the Mix Asymmetric panel of Fig. 3. We use the same vertical profile given in Eq. (19), but we multiply the western profile by 0.7 and the eastern profile by 1.3, so that the horizontally averaged density profile remains the same as in the Bowl-MixSymmetric simulation, but there is an east–west asymmetry. This choice is a crude attempt to mimic the variability in mixing profiles observed in the real ocean. In particular, we were inspired by the iconic mixing profiles reported by Polzin et al. (1997) from the Brazil Basin, where the turbulent density flux was shown to be nearly an order of magnitude larger on the eastern side of the basin than on the western side.

Results from this simulation are quite similar to those with the same mixing profile on the two sides of the basin. The only difference is that the diapycnal velocities (Fig. 7) and turbulent diffusivities (Fig. 6d and Fig. 8, right panel) along the eastern boundary are about twice those along the western boundary, both in the interior and in the BBL, consistent with our choice of imposing a turbulent density flux divergence twice as large in the eastern side than in the western side. We infer that, in an ocean with variable mixing profiles, both the interior sinking and the BBL upwelling are going to be most intense above rough boundaries where the turbulent density flux divergence is largest.

5. Mixing and water mass transformations in the global ocean

De Lavergne et al. (2016) have recently estimated the water mass transformation induced by mixing in the stratified ocean interior. Here, we revisit their result by focusing on the crucial role played by the BBLs. De Lavergne and collaborators considered the contribution of geothermal heat flux and mixing generated by topographic waves breaking locally and nonlocally, that is, close and far from where they were generated. We start our analysis by considering local mixing generated by topographic waves following Nikurashin and Ferrari (2013). We neglect mixing induced by wind-generated waves, which dominate mixing in the upper ocean,

because our focus is on the abyssal water mass transformations close to the bottom topography. Changes in bathymetry are most pronounced below 2000 m, as we show below, and this is where we expect upwelling along BBLs. Extending Nikurashin and Ferrari (2013), we explicitly compute the impact of the interior transformation within the BBLs and show that, consistent with our theoretical analysis, the BBL transformation in the abyssal ocean has the opposite sign and is substantially larger than the overall interior transformation.

Abyssal mixing in the stratified ocean above the BBL is driven by breaking internal waves. These waves are primarily generated by tidal and geostrophic currents flowing over irregular bottom topography (Polzin et al. 1997; St. Laurent et al. 2012). Nikurashin and Ferrari (2013) used linear wave theory to estimate the energy radiated into topographic internal waves and then assumed that ⅓ of that energy was locally dissipated through wave breaking. By further assuming that only ⅙ of the total energy lost in a breaking wave ends up mixing the fluid[3] (Osborn 1980) and that it generates a turbulent density flux that decays exponentially with height above the bottom topography (Jayne and St. Laurent 2001), they generated a map of the turbulent density flux at the top of the BBL, $F_b(x, y)$. The full column turbulent density flux was then estimated by substituting $F_b(x, y)$ in Eq. (18) with an e-folding scale of $d = 500\,\mathrm{m}$, $F_t = 0\,\mathrm{kg\,m^{-2}\,s^{-1}}$.

Nikurashin and Ferrari (2013) computed the water mass transformation using their turbulent density flux map with Eq. (7) but replaced density with neutral density (Jackett and McDougall 1997), a variable that conveniently eliminates irrelevant compressive effects from the full density (an important correction when dealing with the seawater nonlinear equation of state). Their map had a vertical resolution of 250 m below 1500 m, the depth range of interest here. The result of their calculation is shown as blue bars in Fig. 9 and suggests that stratified waters above the BBL are transformed to denser classes by breaking waves, as expected for a density profile decreasing upward.[4] Notice that our focus is on density classes greater than approximately $28.0\,\mathrm{kg\,m^{-3}}$, which sit below 2000 m, where topographic waves are believed to dominate mixing rates.

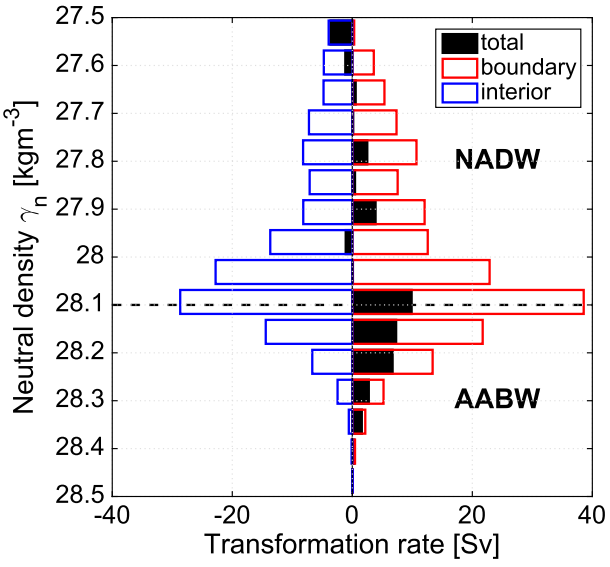

FIG. 9. Water mass transformation for the global ocean based on the estimate of the mixing induced by breaking topographic waves published in Nikurashin and Ferrari (2013). The blue bars indicate the water mass transformation induced by waves breaking in the stratified ocean interior above the BBL. The red bars represent the water mass transformation within the BBL. The solid black bars are the net transformation given by the sum of the interior and BBL transformations. The water mass transformations are plotted as a function of neutral density. The dashed line indicates the $28.1\,\mathrm{kg\,m^{-3}}$ neutral density surface that separates the two major water masses within the density range considered: AABW and NADW.

We extend the Nikurashin and Ferrari (2013) map by imposing that the turbulent density flux goes linearly to zero over the last grid point. This is tantamount to assuming that the turbulent density flux goes from zero to its interior value across a 250-m-deep BBL. The water mass transformation over the BBL is given as red bars in Fig. 9 and confirms that waters become lighter along the BBL. The sum of the negative interior and positive BBL transformations represent the net overturning circulation shown as black bars in Fig. 9. Much like in our idealized simulations, the maximum net deep overturning of about 10 Sv across the neutral density $\gamma = 28.1\,\mathrm{kg\,m^{-3}}$ is a small residual between nearly 40 Sv of waters rising along the boundaries and nearly 30 Sv of waters sinking in the stratified interior.

Figure 10b shows the profile of the area-integrated turbulent density flux across neutral density surfaces based on the estimate of Nikurashin and Ferrari (2013), which was used to generate Fig. 9. The dashed line represents the integral taken over the whole area of each neutral density surface. The continuous line is the

[3] Osborn (1980) argued that $F_\rho^{(z)} \sim 0.2\epsilon$. This relationship can then be used to estimate what fraction of the total energy lost by a wave goes into mixing because $P = \epsilon + F_\rho^{(z)}$ and hence $F_\rho^{(z)} \approx 1/6P$.

[4] Nikurashin and Ferrari (2013) misinterpreted their calculation of the water mass transformation in the stratified interior and incorrectly stated that their calculation implied diabatic rising, rather than sinking, of abyssal waters.

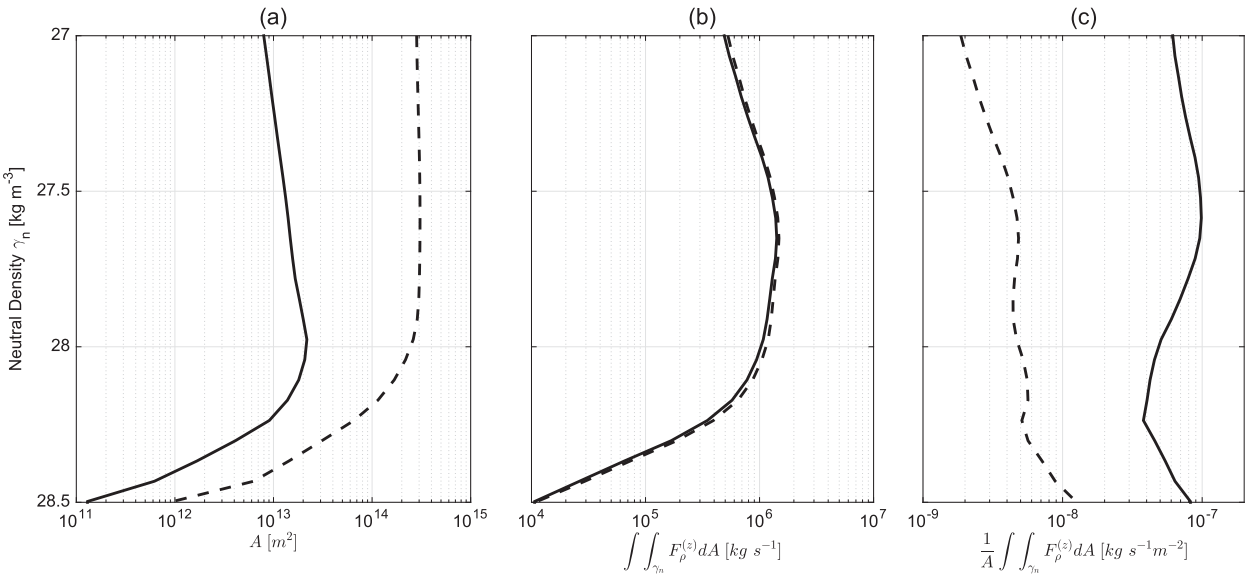

FIG. 10. (a) The total area A of ocean isopycnals and the $A_{\rm mix}$ portion of that area near the ocean boundaries where isopycnals experience the bottom-enhanced mixing; $A_{\rm mix}$ is defined as the portion of the isopycnal area where the turbulent density flux divergence is larger than $1.1 \times 10^{-8}\,{\rm kg\,m^{-3}\,s^{-1}}$. The turbulent density flux is based on the flux estimates of Nikurashin and Ferrari (2013). Only neutral densities higher than $27.0\,{\rm kg\,m^{-3}}$ are considered. (b) The turbulent density flux integrated over $A_{\rm mix}$ and A. (c) The turbulent density flux averaged over $A_{\rm mix}$ and A.

integral taken only over $A_{\rm mix}$, defined as the isopycnal area where the turbulent density flux divergence is larger than $1.1 \times 10^{-11}\,{\rm kg\,m^{-3}\,s^{-1}}$, the value of the globally averaged turbulent density flux 1000 m above the bottom. The two lines are very close, confirming that the topographic mixing is confined to $A_{\rm mix}$. The integral of the turbulent density flux increases toward lighter waters up to $28.0\,{\rm kg\,m^{-3}}$, consistent with upwelling of those waters as per Eq. (8) and Fig. 9. The turbulent density flux changes are smaller for lighter waters and thus we do not expect topographic wave breaking to drive strong flows there, as confirmed in Fig. 9.

Figure 10a plots the vertical profile of the area of near-boundary mixing $A_{\rm mix}$ (solid line). This area represents the near-boundary strip of an isopycnal surface that experiences bottom-enhanced mixing. The along-boundary strip extends from a few tens to a few hundreds of kilometers from the solid boundary to the interior.[5] Topographic roughness on scales less than $O(10)$ km contributes some fuzziness at the edges of $A_{\rm mix}$ but does not affect the overall area. The calculation of $A_{\rm mix}$ is based on the ETOPO5 (National Geophysical Data Center 1993) global 5-min topography, which is reasonably accurate at scales larger than 10 km. The major uncertainty in the calculation is likely to arise from unknown variations in the e-folding scale of mixing.

The area $A_{\rm mix}$ increases by two orders of magnitude between the ocean bottom and the neutral density $28.0\,{\rm kg\,m^{-3}}$, and it is a full order of magnitude smaller than the full ocean area (dashed line). Densities larger than $28.0\,{\rm kg\,m^{-3}}$ correspond to Antarctic Bottom Water and the densest North Atlantic Deep Water. We thus expect that topographic effects and BBL upwelling will be most important for these deep waters and less above. The rapid increase in $A_{\rm mix}$ is primarily associated with the increase of the arc length of the bathymetry as one moves upward in the water column up to approximately 2000 m. At shallower depths, $A_{\rm mix}$ remains approximately constant because the majority of ridges and seamounts in the ocean do not reach above 2000 m.

Finally, in Fig. 10c, we show the turbulent density flux averaged (not integrated) over $A_{\rm mix}$ (solid line) and averaged over the whole isopycnal area (dashed line). The area-averaged turbulent density flux decreases by at most a factor of 5 between the bottom and the $28.0\,{\rm kg\,m^{-3}}$ isopycnal, while the area $A_{\rm mix}$ drops by two orders of magnitude over the same depth range. According to Eq. (9), this implies that the net upwelling of

[5] Equation (10) shows that the width of $A_{\rm mix}$ is given by the ratio of the e-folding scale of the turbulent density flux over the tangent of the topographic slope, measured on scales larger than 10 km, that is, scales larger than those of the waves that are radiated from the topography and generate the mixing. For a typical e-folding scale of 500 m and a mild topographic slope of $1/400$, we infer a width of 200 km [setting $\alpha = 1$ in Eq. (10)]. Steeper slopes would result in a narrower $A_{\rm mix}$.

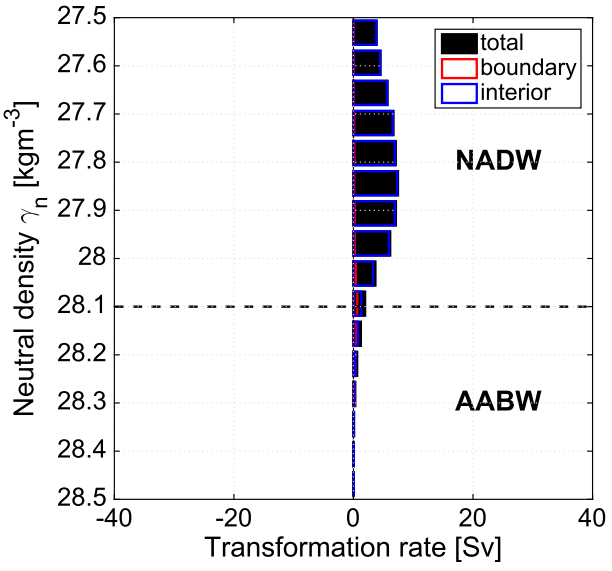

FIG. 11. Water mass transformation for the global ocean induced by background mixing represented as a turbulent density flux $F_\rho^{(z)} = -\kappa \partial_z \gamma$, where κ is a constant background diffusivity of $10^{-5}\,\mathrm{m^2\,s^{-1}}$. The blue bars indicate the water mass transformation induced by waves breaking in the ocean interior above the BBL. The red bars represent the water mass transformation within the BBL. The solid black bars are the net transformation given by the sum of the interior and BBL transformations. Nearly all the transformation occurs in the stratified interior. The water mass transformations are plotted as a function of neutral density γ for the same range used in Fig. 9. The dashed line indicates the $28.1\,\mathrm{kg\,m^{-3}}$ neutral density surface that separates the two major water masses in this density range: AABW and NADW.

waters denser than $28.0\,\mathrm{kg\,m^{-3}}$ is primarily a result of the increase in the area of near-topography mixing.

A full study of water mass transformations in the deep ocean should include the effect of mixing associated with internal waves generated locally and nonlocally. The turbulent density flux map produced by Nikurashin and Ferrari (2013) considered only mixing associated with topographic waves that break locally near their generation sites. De Lavergne et al. (2016) attempted to estimate the mixing associated with nonlocal waves, but their results were quite uncertain. To get a sense of the overall importance of these nonlocal waves in driving diapycnal flows in the abyss, we appeal to the observational evidence that, away from regions where strong topographic waves are generated, ocean mixing is weak and characterized by a background turbulent diffusivity of about $10^{-5}\,\mathrm{m^2\,s^{-1}}$ (Waterhouse et al. 2014). Figure 11 shows the water mass transformation calculated with Eq. (7) and a turbulent density flux given by $F_\rho^{(z)} = -\kappa \partial_z \gamma$ with $\kappa = 1.0 \times 10^{-5}\,\mathrm{m^2\,s^{-1}}$ and $\partial_z \gamma$ based on the WOCE hydrographic map of neutral density γ (Gouretski and Koltermann 2004). The background mixing contributes little diapycnal upwelling for waters denser than $28.0\,\mathrm{kg\,m^{-3}}$, where topographic waves dominate and stratification is weak, but it becomes dominant for the more stratified lighter waters. Diapycnal upwelling along BBLs is confined to Antarctic Bottom Water and the densest North Atlantic Deep Water, where mixing is bottom intensified and the length of incrop lines increases upward. For waters lighter than $28.0\,\mathrm{kg\,m^{-3}}$, diapycnal upwelling is more uniformly distributed throughout the ocean interior.

It should be clear that our global estimate of the water mass transformation is very uncertain, as it relies on a poorly constrained estimate of the turbulent density fluxes induced by mixing. But the pattern of sinking in the interior and upwelling along the abyssal BBLs is robust because it depends only on having a turbulent density flux decreasing upward above the BBL, as suggested by many independent observations (Polzin et al. 1997; St. Laurent et al. 2012; Waterman et al. 2013; Waterhouse et al. 2014), and a turbulent density flux going to zero in the BBL, as demanded by the no flux boundary condition through the ocean bottom.

De Lavergne et al. (2016) studied the effect of the geothermal heat flux in their analysis, which we ignored, and showed that it lightens waters along the ocean boundaries and drives a few additional Sverdrups to the total BBL transport. Based on the work presented in this paper, this implies that the geothermal heat flux further reinforces the diapycnal upwelling of bottom waters along the BBLs. De Lavergne et al. (2016) also considered the effects of nonlinearities in the equation of state of seawater, which we ignored, and found that those effects introduce minor corrections.

6. Conclusions

The global overturning circulation is thought to consist of sinking of dense waters at high latitudes, a concentrated upwelling in the latitude band of the Southern Ocean and a broader upwelling spread across all ocean basins. The upwelling in the Southern Ocean is along isopycnals and driven by the surface westerlies. The upwelling in the basins crosses density surfaces (i.e., it is a diapycnal upwelling) and has been thought to be associated with widespread mixing as first proposed by Munk (1966) in his seminal paper on abyssal recipes. In this manuscript, we have shown that the recent observational evidence that mixing is most intense close to the ocean bottom is inconsistent with this picture. The observed vertical profile of mixing drives diapycnal sinking of deep waters toward the abyss in the ocean interior. We have argued that the diapycnal upwelling of waters is instead confined to thin, turbulent boundary layers

along the sloping ocean boundaries. The boundary layer diapycnal upwelling must be so intense as to overcome the interior diapycnal sinking and allow waters to rise toward the surface in the net. This hypothesis has been illustrated with theory, idealized simulations, and a global map of ocean mixing.

Our result applies to the abyssal density layers that outcrop only in the Southern Ocean and across which waters upwell diapycnally in the ocean interior. Density surfaces that outcrop both in the North Atlantic and in the Southern Ocean have flow mostly along density surfaces and are believed to respond more to surface wind patterns and air–sea fluxes than to interior mixing. Also, mixing profiles are observed to decay rapidly above the bottom in regions with rough topography and intense wave breaking, while the mixing profiles are more uniform over abyssal plains. We thus expect boundary diapycnal upwelling to be concentrated along rough boundaries rather than along smooth ones.

Our work differs in a fundamental way from previous investigations that emphasized the role of enhanced mixing along the ocean boundaries on the ocean overturning circulation (Scott and Marotzke 2002; Spall 2001). In our study, the focus is not on the enhancement of mixing along the boundaries; rather, we are emphasizing the decrease in mixing within the bottom boundary layers that drive the upwelling of abyssal waters. Our work differs also from the literature on diffusion-driven flows along sloping boundaries (Garrett et al. 1993). That literature investigates the flows that arise within a boundary in response to local mixing, while we illustrate how the boundaries accommodate the rising of waters that sink in response to bottom-intensified mixing in the stratified interior.

St. Laurent et al. (2001) and Thurnherr et al. (2005) diagnosed the overturning circulation for the Brazil Basin using an inverse model together with vertical profiles of temperature, salinity, and turbulence collected as part of the Brazil Basin Tracer Release Experiment. They inferred that waters sunk away from boundaries in response to the interior mixing, while they upwelled along the rough boundary of the Mid-Atlantic Ridge. Polzin (2009) confirmed this overall picture with a theoretical study of the depth profile of turbulent dissipation in the region. Here, we have generalized these results to the global ocean, emphasizing the importance of the ocean's bathymetry or more precisely the length of density incrop lines as a function of density in determining whether the along-boundary upwelling exceeds the interior sinking.

Our results have important implications for the horizontal abyssal circulation in addition to the overturning. Stommel, Arons, and Faller in a series of papers from 1958 to 1960 laid the foundation for our present understanding of the horizontal abyssal circulation (Stommel 1958; Stommel et al. 1958; Stommel and Arons 1960). They argued that mixing drives a pervasive diapycnal upwelling of waters from the abyss, resulting in a stretching of water columns within all ocean basins. This stretching in turn would force waters to flow poleward to conserve their potential vorticity and to return equatorward along deep western boundary currents. McDougall (1989) and Rhines (1993) pointed out that sloping boundaries modify this picture. Our argument that ocean waters sink across density surfaces in response to mixing in the stratified ocean interior and rise along lateral boundaries results in an even more complex geometry of squeezing and stretching of water columns, further modifying the overall deep gyre circulation. There is a lot more to understand about this new emerging view of the ocean abyssal circulation.

An interesting puzzle emerging from our work is whether large-scale numerical models capture the dichotomy of diapycnal sinking of ocean waters in the stratified interior and diapycnal rising along the boundaries. Numerical models used for climate studies typically represent mixing with a prescribed vertical diffusivity profile either constant or small in the upper ocean and large below about 2000 m (Bryan and Lewis 1979). With both choices, the resulting turbulent density flux profile $F_\rho^{(z)} = -\kappa\partial_z\rho$ is likely to decrease toward the ocean bottom where the stratification $\partial_z\rho$ is small. Thus, in these numerical models, waters are expected to rise rather than sink diapycnally in the stratified abyssal ocean interior, with implications for both the transport of tracers and the abyssal circulation. More recent models that use a κ profile that increases toward the ocean bottom (e.g., Simmons et al. 2004; Saenko and Merryfield 2005; Melet et al. 2012, 2015) may reproduce the right flow structure as long as the bottom increase in κ overwhelms the bottom decrease in stratification. Observations suggest that the vertical divergence of the turbulent density flux in the abyssal ocean $\partial_z F_\rho^{(z)} = -(\partial_z\kappa)(\partial_z\rho) - \kappa\partial_z^2\rho$ is dominated by the decrease in diffusivity away from the ocean bottom, $(\partial_z\kappa)(\partial_z\rho) > 0$, and not by the increase in stratification, $\kappa\partial_z^2\rho < 0$. It is not clear whether existing parameterizations result in a sufficient bottom enhancement of κ to generate bottom-enhanced $F_\rho^{(z)}$ profiles.

To conclude, we believe that our results call for detailed observational programs of the flows and mixing in the turbulent bottom boundary layers. There are hardly any observations of the turbulent fluxes in the bottom boundary layers of the ocean abyss, while there are more observations of deep-ocean mixing in the stratified interior. A full picture of the global ocean overturning

requires sampling of turbulence and the vertical motions in both regions.

Acknowledgments. The work benefitted from discussions with Carl Wunsch and Joern Callies and email exchanges with Chris Garrett, Andrew Hogg, and Gurvan Madec. Matthew Alford generously shared an unpublished manuscript on observational estimates of the sinking induced by mixing in the abyssal ocean. Louise Bell is thanked for preparing the first two illustrations. We gratefully acknowledge National Science Foundation support through Award OCE-1233832 (R.F.) and Australian Research Council support though Grant DE150100937.

REFERENCES

Armi, L., 1978: Some evidence for boundary mixing in the deep ocean. *J. Geophys. Res.*, **83**, 1971–1979, doi:10.1029/JC083iC04p01971.

Bouffard, D., and L. Boegman, 2013: A diapycnal diffusivity model for stratified environmental flows. *Dyn. Atmos. Oceans*, **61–62**, 14–34, doi:10.1016/j.dynatmoce.2013.02.002.

Bryan, K., and J. L. Lewis, 1979: A water mass model of the world ocean. *J. Geophys. Res.*, **84**, 2503–2517, doi:10.1029/JC084iC05p02503.

de Lavergne, C., G. Madec, J. Le Sommer, G. A. J. Nurser, and A. C. Naveira Garabato, 2016: On the consumption of Antarctic Bottom Water in the abyssal ocean. *J. Phys. Oceanogr.*, **46**, 635–661, doi:10.1175/JPO-D-14-0201.1.

Ferrari, R., 2014: Oceanography: What goes down must come up. *Nature*, **513**, 179–180, doi:10.1038/513179a.

Ganachaud, A., and C. Wunsch, 2000: Improved estimates of global ocean circulation, heat transport and mixing from hydrographic data. *Nature*, **408**, 453–457, doi:10.1038/35044048.

Gargett, A. E., 1984: Vertical eddy diffusivity in the ocean interior. *J. Mar. Res.*, **42**, 359–393, doi:10.1357/002224084788502756.

Garrett, C., 1990: The role of secondary circulation in boundary mixing. *J. Geophys. Res.*, **95**, 3181–3188, doi:10.1029/JC095iC03p03181.

——, and E. Kunze, 2007: Internal tide generation in the deep ocean. *Annu. Rev. Fluid Mech.*, **39**, 57–87, doi:10.1146/annurev.fluid.39.050905.110227.

——, P. MacCready, and P. Rhines, 1993: Boundary mixing and arrested Ekman layers: Rotating stratified flow near a sloping boundary. *Annu. Rev. Fluid Mech.*, **25**, 291–323, doi:10.1146/annurev.fl.25.010193.001451.

——, K. Speer, and E. Tragou, 1995: The relationship between water mass transformation and the surface buoyancy flux with application to Phillip's Red Sea model. *J. Phys. Oceanogr.*, **25**, 1696–1705, doi:10.1175/1520-0485(1995)025<1696:TRBWMF>2.0.CO;2.

Gent, P. R., and J. C. McWilliams, 1990: Isopycnal mixing in ocean circulation models. *J. Phys. Oceanogr.*, **20**, 150–155, doi:10.1175/1520-0485(1990)020<0150:IMIOCM>2.0.CO;2.

Gouretski, V., and K. Koltermann, 2004: WOCE global hydrographic climatology: A technical report. Berichte des Bundesamtes für Seeschifffahrt und Hydrographie 35/2004, 52 pp.

Gregg, M. C., 1987: Diapycnal mixing in the thermocline. *J. Geophys. Res.*, **92**, 5249–5286, doi:10.1029/JC092iC05p05249.

Jackett, D. R., and T. J. McDougall, 1997: A neutral density variable for the world's oceans. *J. Phys. Oceanogr.*, **27**, 237–263, doi:10.1175/1520-0485(1997)027<0237:ANDVFT>2.0.CO;2.

Jayne, S. R., and L. C. St. Laurent, 2001: Parameterizing tidal dissipation over rough topography. *Geophys. Res. Lett.*, **28**, 811–814, doi:10.1029/2000GL012044.

Karimpour, F., and S. K. Venayagamoorthy, 2014: A simple turbulence model for stably stratified wall-bounded flows. *J. Geophys. Res. Oceans*, **119**, 870–880, doi:10.1002/2013JC009332.

Klocker, A., and T. J. McDougall, 2010: Quantifying the consequences of the ill-defined nature of neutral surfaces. *J. Phys. Oceanogr.*, **40**, 1866–1880, doi:10.1175/2009JPO4212.1.

Kunze, E., C. MacKay, E. E. McPhee-Shaw, K. Morrice, J. B. Girton, and S. R. Terker, 2012: Turbulent mixing and exchange with interior waters on sloping boundaries. *J. Phys. Oceanogr.*, **42**, 910–927, doi:10.1175/JPO-D-11-075.1.

Lumpkin, R., and K. Speer, 2007: Global ocean meridional overturning. *J. Phys. Oceanogr.*, **37**, 2550–2562, doi:10.1175/JPO3130.1.

Marshall, J., and T. Radko, 2003: Residual-mean solutions for the Antarctic Circumpolar Current and its associated overturning circulation. *J. Phys. Oceanogr.*, **33**, 2341–2354, doi:10.1175/1520-0485(2003)033<2341:RSFTAC>2.0.CO;2.

——, and K. Speer, 2012: Closure of the meridional overturning circulation through southern ocean upwelling. *Nat. Geosci.*, **5**, 171–180, doi:10.1038/ngeo1391.

——, A. Adcroft, C. Hill, L. Perelman, and C. Heisey, 1997: A finite-volume, incompressible Navier Stokes model for studies of the ocean on parallel computers. *J. Geophys. Res.*, **102**, 5753–5766, doi:10.1029/96JC02775.

——, D. Jamous, and J. Nilsson, 1999: Reconciling thermodynamic and dynamic methods of computation of water-mass transformation rates. *Deep-Sea Res. I*, **46**, 545–572, doi:10.1016/S0967-0637(98)00082-X.

Mashayek, A., and W. R. Peltier, 2013a: Shear-induced mixing in geophysical flows: Does the route to turbulence matter to its efficiency? *J. Fluid Mech.*, **725**, 216–261, doi:10.1017/jfm.2013.176.

——, and ——, 2013b: Time-dependent, non-monotonic mixing in stratified turbulent shear flows: Implications for oceanographic estimates of buoyancy flux. *J. Fluid Mech.*, **736**, 570–593, doi:10.1017/jfm.2013.551.

——, R. Ferrari, M. Nikurashin, and W. R. Peltier, 2015: Influence of enhanced abyssal diapycnal mixing on ocean stratification and overturning circulation. *J. Phys. Oceanogr.*, **45**, 2580–2597, doi:10.1175/JPO-D-15-0039.1.

McDougall, T. J., 1984: The relative roles of diapycnal and isopycnal mixing on subsurface water mass conversion. *J. Phys. Oceanogr.*, **14**, 1577–1589, doi:10.1175/1520-0485(1984)014<1577:TRRODA>2.0.CO;2.

——, 1989: Dianeutral advection. *Parameterization of Small-Scale Processes: Proc. 'Aha Huliko'a Hawaiian Winter Workshop*, Honolulu, HI, University of Hawai'i at Mānoa, 289–315.

Melet, A., R. Hallberg, S. Legg, and K. Polzin, 2012: Sensitivity of the ocean state to the vertical distribution of internal-tide-driven mixing. *J. Phys. Oceanogr.*, **43**, 602–615, doi:10.1175/JPO-D-12-055.1.

——, ——, A. Adcroft, M. Nikurashin, and S. Legg, 2015: Energy flux into internal lee waves: Sensitivity to future climate changes using linear theory and a climate model. *J. Climate*, **28**, 2365–2384, doi:10.1175/JCLI-D-14-00432.1.

Munday, D. R., H. L. Johnson, and D. P. Marshall, 2013: Eddy saturation of equilibrated circumpolar currents. *J. Phys. Oceanogr.*, **43**, 507–532, doi:10.1175/JPO-D-12-095.1.

Munk, W., 1966: Abyssal recipes. *Deep-Sea Res. Oceanogr. Abstr.*, **13**, 707–730, doi:10.1016/0011-7471(66)90602-4.

——, 1981: Internal waves and small-scale processes. *Evolution of Physical Oceanography*, B. A. Warren and C. Wunsch, Eds., MIT Press, 264–291.

——, and C. Wunsch, 1998: Abyssal recipes II: Energetics of tidal and wind mixing. *Deep-Sea Res. I*, **45**, 1977–2010, doi:10.1016/S0967-0637(98)00070-3.

National Geophysical Data Center, 1993: 5-minute Gridded Global Relief Data (ETOPO5). National Geophysical Data Center, doi:10.7289/V5D798BF.

Nikurashin, M., and G. Vallis, 2011: A theory of deep stratification and overturning circulation in the ocean. *J. Phys. Oceanogr.*, **41**, 485–502, doi:10.1175/2010JPO4529.1.

——, and R. Ferrari, 2013: Overturning circulation driven by breaking internal waves in the deep ocean. *Geophys. Res. Lett.*, **40**, 3133–3137, doi:10.1002/grl.50542.

Nurser, A., and M.-M. Lee, 2004: Isopycnal averaging at constant height. Part II: Relating to the residual streamfunction in Eulerian space. *J. Phys. Oceanogr.*, **34**, 2740–2755, doi:10.1175/JPO2650.1.

Oka, A., and Y. Niwa, 2013: Pacific deep circulation and ventilation controlled by tidal mixing away from the sea bottom. *Nat. Commun.*, **4**, 1–8, doi:10.1038/ncomms3419.

Osborn, T. R., 1980: Estimates of the local rate of vertical diffusion from dissipation measurements. *J. Phys. Oceanogr.*, **10**, 83–89, doi:10.1175/1520-0485(1980)010<0083:EOTLRO>2.0.CO;2.

Peltier, W. R., and C. P. Caulfield, 2003: Mixing efficiency in stratified shear flows. *Annu. Rev. Fluid Mech.*, **35**, 135–167, doi:10.1146/annurev.fluid.35.101101.161144.

Polzin, K. L., 2009: An abyssal recipe. *Ocean Modell.*, **30**, 298–309, doi:10.1016/j.ocemod.2009.07.006.

——, J. M. Toole, J. R. Ledwell, and R. W. Smith, 1997: Spatial variability of turbulent mixing in the abyssal ocean. *Science*, **276**, 93–96, doi:10.1126/science.276.5309.93.

Rhines, P., 1993: Oceanic general circulation: Wave and advection dynamics. *Modelling Oceanic Climate Interactions*, J. Willebrand and D. L. T. Anderson, Eds., NATO ASI Subseries I, Vol. 11, Springer-Verlag, 67–149.

Saenko, O. A., and W. J. Merryfield, 2005: On the effect of topographically enhanced mixing on the global ocean circulation. *J. Phys. Oceanogr.*, **35**, 826–834, doi:10.1175/JPO2722.1.

Scott, J. R., and J. Marotzke, 2002: The location of diapycnal mixing and the meridional overturning circulation. *J. Phys. Oceanogr.*, **32**, 3578–3595, doi:10.1175/1520-0485(2002)032<3578:TLODMA>2.0.CO;2.

Simmons, H. L., S. R. Jayne, L. C. Laurent, and A. J. Weaver, 2004: Tidally driven mixing in a numerical model of the ocean general circulation. *Ocean Modell.*, **6**, 245–263, doi:10.1016/S1463-5003(03)00011-8.

Smyth, W. D., J. N. Moum, and D. R. Caldwell, 2001: The efficiency of mixing in turbulent patches: Inferences from direct simulations and microstructure observations. *J. Phys. Oceanogr.*, **31**, 1969–1992, doi:10.1175/1520-0485(2001)031<1969:TEOMIT>2.0.CO;2.

Spall, M. A., 2001: Large-scale circulations forced by localized mixing over a sloping bottom. *J. Phys. Oceanogr.*, **31**, 2369–2384, doi:10.1175/1520-0485(2001)031<2369:LSCFBL>2.0.CO;2.

St. Laurent, L. C., J. M. Toole, and R. W. Schmitt, 2001: Buoyancy forcing by turbulence above rough topography in the abyssal Brazil Basin. *J. Phys. Oceanogr.*, **31**, 3476–3495, doi:10.1175/1520-0485(2001)031<3476:BFBTAR>2.0.CO;2.

——, A. C. Naveira Garabato, J. R. Ledwell, A. M. Thurnherr, J. M. Toole, and A. J. Watson, 2012: Turbulence and diapycnal mixing in Drake Passage. *J. Phys. Oceanogr.*, **42**, 2143–2152, doi:10.1175/JPO-D-12-027.1.

Stommel, H., 1958: The abyssal circulation. *Deep-Sea Res.*, **5**, 80–82, doi:10.1016/S0146-6291(58)80014-4.

——, and A. B. Arons, 1960: On the abyssal circulation of the world ocean—I. Stationary planetary flow patterns on a sphere. *Deep-Sea Res.*, **6**, 140–154, doi:10.1016/0146-6313(59)90065-6.

——, ——, and A. J. Faller, 1958: Some examples of stationary planetary flow patterns in bounded basins. *Tellus*, **10A**, 179–187, doi:10.1111/j.2153-3490.1958.tb02003.x.

Talley, L. D., 2013: Closure of the global overturning circulation through the Indian, Pacific, and Southern Oceans: Schematics and transports. *Oceanography*, **26**, 80–97, doi:10.5670/oceanog.2013.07.

——, G. L. Pickard, W. J. Emery, and J. H. Swift, 2011: *Descriptive Physical Oceanography: An Introduction.* 6th ed. Academic Press, 555 pp.

Thorpe, S. A., 1982: On the layers produced by rapidly oscillating a vertical grid in a uniformly stratified fluid. *J. Fluid Mech.*, **124**, 391–409, doi:10.1017/S0022112082002559.

Thurnherr, M., L. C. St. Laurent, K. G. Speer, J. M. Toole, and J. R. Ledwell, 2005: Mixing associated with sills in a canyon on the midocean ridge flank. *J. Phys. Oceanogr.*, **35**, 1370–1381, doi:10.1175/JPO2773.1.

Walin, G., 1982: On the relation between sea-surface heat flow and thermal circulation in the ocean. *Tellus*, **34A**, 187–195, doi:10.1111/j.2153-3490.1982.tb01806.x.

Waterhouse, A. F., and Coauthors, 2014: Global patterns of diapycnal mixing from measurements of the turbulent dissipation rate. *J. Phys. Oceanogr.*, **44**, 1854–1872, doi:10.1175/JPO-D-13-0104.1.

Waterman, S., A. C. Naveira Garabato, and K. L. Polzin, 2013: Internal waves and turbulence in the Antarctic Circumpolar Current. *J. Phys. Oceanogr.*, **43**, 259–282, doi:10.1175/JPO-D-11-0194.1.

Weatherly, G. L., and P. J. Martin, 1978: On the structure and dynamics of the oceanic bottom boundary layer. *J. Phys. Oceanogr.*, **8**, 557–570, doi:10.1175/1520-0485(1978)008<0557:OTSADO>2.0.CO;2.

Wolfe, C. L., and P. Cessi, 2011: The adiabatic pole-to-pole overturning circulation. *J. Phys. Oceanogr.*, **41**, 1795–1810, doi:10.1175/2011JPO4570.1.

Wunsch, C., 1970: On oceanic boundary mixing. *Deep-Sea Res. Oceanogr. Abstr.*, **17**, 293–301, doi:10.1016/0011-7471(70)90022-7.

——, and R. Ferrari, 2004: Vertical mixing, energy, and the general ocean circulation. *Annu. Rev. Fluid Mech.*, **36**, 281–314, doi:10.1146/annurev.fluid.36.050802.122121.

——, and P. Heimbach, 2009: The global zonally integrated ocean circulation, 1992–2006: Seasonal and decadal variability. *J. Phys. Oceanogr.*, **39**, 351–368, doi:10.1175/2008JPO4012.1.